Preparation, Characterization and Testing for Photocatalytic Activities of Bi_2WO_6-based Materials

By Hanna Qin

At thesis submitted to the
Faculty of Graduate and Postdoctoral Studies
in partial fulfillment of the requirements for the degree of

Master of Applied Science, Chemical Engineering

Under the auspices of the Department of Chemical & Biological Engineering

University of Ottawa
Ottawa, Ontario, Canada
November 2012

Abstract

$PdCl_2/Bi_2WO_6$ and Pd/Bi_2WO_6 composite photocatalysts were synthesized via a template free hydrothermal process and the respective photocatalytic activities were investigated by degradation of Rhodamine B. The new catalyst composites were characterized by X-ray diffraction (XRD), scanning electron microscopy (SEM), X-ray photoelectron spectroscopy (XPS) and ultraviolet visible (UV-vis) light diffuse reflectance spectra, respectively. By XRD, it was found that the loaded Pd species did not alter the crystal lattice of Bi_2WO_6 photocatalyst. Through the XPS spectra, it was found that the $PdCl_2/Bi_2WO_6$ was successfully reduced by chemical reducing agents CH_2O and N_2H_4, respectively, and palladium was present in the form of both metallic Pd and Pd ion species (Pd^0 and Pd^{2+}), while the Pd species in a $NaBH_4$-reduced composite exhibited only metallic Pd species (Pd^0). For the SEM images, it was observed that both classes of composites were constructed from plenty of nanoplates, which were closed packed with hierarchical structures. Furthermore, the removal efficiency of Rhodamine B was found to be influenced by parameters such as catalyst dosage, pollutant concentration and solution pH.

Résumé

Les photo-catalyseurs composés $PdCl_2/Bi_2WO_6$ et Pd/Bi_2WO_6 furent synthétisés suivant un procédé hydrotermique, et leurs activités photo-catalytiques mesurées par l'analyse de la dégradation de Rhodamine B. Les photo-catalyseurs composés furent caractérisés par diffractométrie à rayon X (DRX), microscopie électronique à balayage (MEB), spectrométrie photoélectronique X (XPS) et par l'analyse des spectres de réflexion de lumière ultraviolette/visible (UV-vis). D'après les résultats de DRX, il fut déterminé que la présence de Pd n'altère pas la structure du réseau cristallin du photo-catalyseur Bi_2WO_6. L'analyse des spectres XPS indique que le Pd/Bi_2WO_6 fut réduit par les agents réducteurs CH_2O et N_2H_4, et le Pd fut présent sous ses conditions sous ses formes métalliques et ioniques (Pd^0 and Pd^{2+}), tandis qu'en présence de $NaBH_4$, il n'est présent que sous sa forme métallique (Pd^0). Les images obtenues par MEB démontrent que les deux photo-catalyseurs sont composés d'une multitude de nanoplaques, organisées selon un agencement serré composé de structures hiérarchiques. L'efficacité de dégradation de Rhodamine B fut affectée par certains paramètres, notamment la dose de catalyseur utilisée, la concentration du polluant, et le pH de la solution.

Acknowledgment

I take great pleasure in thanking the many people who have helped me in my studies at the University of Ottawa. First and foremost, I would like to express my sincere appreciation and deep thanks to my supervisor, Dr Jason Zhang, for giving me the opportunity to complete a master's degree in chemical engineering under his guidance. His encouragement and advice greatly helped me in both my research and in writing this thesis.

I also would like to thank Dr. Wenquan Cui, and Joanne Gamage for their stimulating discussion and assistance throughout my research project.

I am grateful to the technical staffs from the department and the professors from material characterization core center, who helped me to do the material characterization tests for my samples.

Finally, I would like to extend my thanks to my parents and my colleagues, whose encouragement have always sustained me.

Table of Contents

List of Figures

List of Tables

Nomenclature

VLD	visible light driven
RhB	Rhodamine B
XRD	X-ray diffraction
XPS	X-ray photoelectron spectroscopy
SEM	scanning electron microscopy
UV-vis	ultraviolet and visible

Chapter 1. Introduction

1.1. Background

In the past decades, interest focused on photocatalysis for environmental and energy-related applications have resulted in increased research in this area. The development of an environmentally-friendly photocatalysis process has been considered for application to many systems, including for the efficient degradation of a wide range of organic pollutants and the inactivation of microorganisms under visible light. Figure 1 illustrates some applications of photocatalysis previously reported.

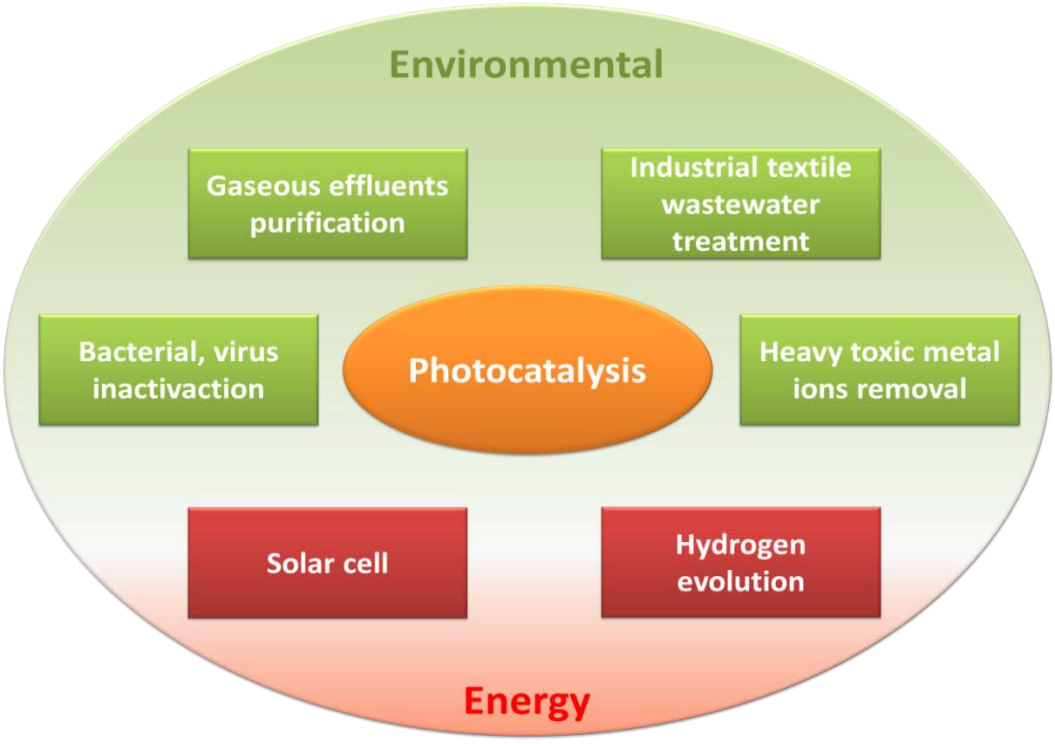

Figure 1 Applications of photocatalysis

Previous studies have demonstrated that Bi_2WO_6 as a photocatalytic material possesses significantly higher optical absorption in the wavelength region above 449 nm than bismuth oxides, such as Bi_2O_3 and $Bi_2W_2O_9$, raising the possibility of enhanced photocatalytic activity using this material under solar illumination, which contains mainly visible light irradiation (43% between 400-700 nm). Bi_2WO_6 has been widely studied and used in many applications due to its unique physical and chemical properties for the improvement of photocatalysis. Its activity has been demonstrated for the efficient decomposition of organic pollutants, and it has been shown to possess chemical stability, long durability, nontoxicity, low cost, and absorption in visible light region.

The photocatalytic activity of Bi_2WO_6 depends on its absorption behaviour, photo-response region and the separation efficiency of photo-generated electron-hole pairs. Accordingly, three predominant approaches have been investigated to enhance the photocatalytic activity of this material. One approach is to extend the specific surface area of Bi_2WO_6 through the use of a controllable synthesis method. The second approach is to increase the photo-response region of Bi_2WO_6 by the introduction of doping ions, transition metals or other semiconductors. The third approach is to maximize the transfer efficiency and to enhance the oxidation power of photogenerated carriers. Noble metals such as Ag, Pt, Ru and Au have been used to improve the electron migration efficiency and restrict the photogenerated electrons and holes recombination. To date, many efforts have been made in improving the photocatalytic activity of Bi_2WO_6-assisted composites. However, there are still some drawbacks associated to these modified materials, which hinder their lifetime and cause a limited absorption in visible light region. To meet the requirements of the future practical applications of Bi_2WO_6 photocatalysts, it is necessary

to design novel Bi_2WO_6-assisted photocatalystic materials which are capable of addressing these issues.

1.2. Project objectives

To address the issues related to poor visible light absorption and quick electron-hole recombination, and to improve visible-light efficiency Bi_2WO_6, the research objectives were defined and are summarized as follows:

1. To synthesize Bi_2WO_6 by a template-free hydro-thermal method, and to load $PdCl_2$ species on the Bi_2WO_6 host material using an isometric impregnation method.
2. To regulate the redox status of loaded Pd by chemical reductants using CH_2O, N_2H_4 and $NaBH_4$.
3. To test photocatalytic activities of the newly prepared catalysts for degradation of Rhodamine B (RhB) under visible light irradiation
4. To study the size, structure, morphology, optical absorption properties and composition of all prepared composites by X-ray diffraction (XRD), X-ray photoelectron spectroscopy (XPS), scanning electron microscopy (SEM) and ultraviolet visible (UV-vis) light diffuse reflectance spectra.

1.3. Thesis outline

The main body of this thesis consists of three chapters, prepared as original research articles. All these papers will be submitted for publication shortly after the thesis defense. It should also be noted that a patent related to the work described herein is also in preparation by the MASc candidate.

Chapter 2 presents a literature review on the work carried out in photocatalysis, and spe-

cifically, reviews the synthesis methods used in literature to prepare Bi_2WO_6 and Bi_2WO_6-composites and examines their photocatalytic applications.

In Chapter 3, the results from studies on the synthesis of $PdCl_2/Bi_2WO_6$ composite materials and their visible light driven photocatalysis are discussed, including structural and mechanistic analysis.

In Chapter 4, the effects of chemical reducing agents on the preparation of Pd/Bi_2WO_6 composite from $PdCl_2/Bi_2WO_6$ are explored, and the visible light driven photocatalysis using the reduced catalysts is investigated.

Finally, in Chapter 5, major conclusions from this research are highlighted, and recommendations for future work are made.

Chapter 2. Literature Review

2.1. Introduction

Due to increased concern over environmental issues related to the traditional use of fossil fuels, attention has been focused on photocatalysis as a treatment and energy generation option in the past three decades. This process is eco-friendly in that it employs inexhaustible sunlight as a renewable source of required photons for the photoinduced processes. Heterogeneous photocatalysis is an advanced oxidation process which has been the subject of a tremendous amount of research related to decomposition of a wide range of organic pollutants, also the photocatalytic inactivation many microorganisms including various types of bacteria, fungi, viruses, and spores. Heterogeneous photocatalysis mainly consists of acceleration of a photoreaction in the presence of a semiconductor photocatalyst, and its major application is in the photocatalytic oxidation (PCO) to effect partial or total mineralization of liquid or gas phase pollutants to benign substances [1]. Of the investigated pollutants, the majority of studies have been focused on organic dye degradation. The early photochemical studies on the degradation of organic dyes in presence of inorganic semiconductors such as silver halides and zinc oxide were driven by applications related to of electron photography [2]. The first example of this from the literature was in the use of inorganic semiconductor to reduce Methylene Blue to the leuco form, and was reported in 1969. Subsequent to this, other studies reported that the Rhodamine B and Methylene Blue could be degraded by CdS photocatalyst under solar irradiation. Around 1980, the photogenerated electrons transfer from titanium oxide to Methyl Or-

ange were observed to result in the reduced absorption of the dye by bleaching. Thereafter, studies were performed investigating the degradation of other organic materials. Table 1 shows the structure of some representative organic dyes that are frequently employed in photocatalytic studies.

Table 1 Structure of some model organic dyes typically employed in photocatalysis studies

Type of dye	**Examples**	**Structure**
Azo	Reactive Orange 16	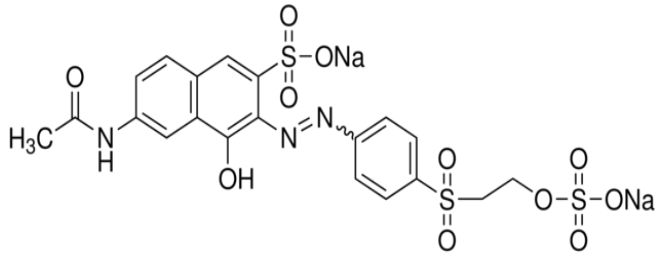
Xanthene	Basic Violet 10	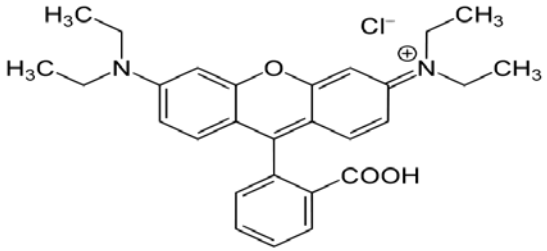
Thiazine	Methylene Blue	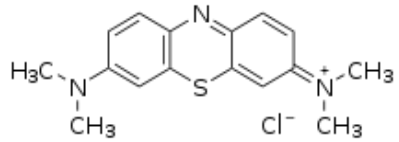

Type of dye	Examples	Structure
Anthraquinone	Rective Blue 4	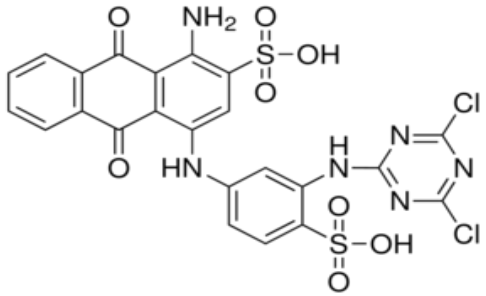
Indigo	Indigo Carmine	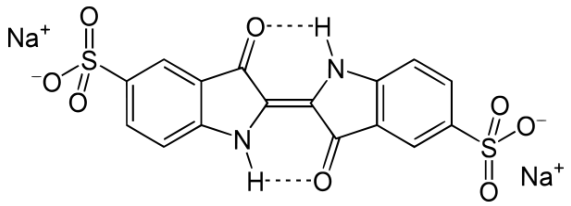
Phenanthrene	D&C Green 8	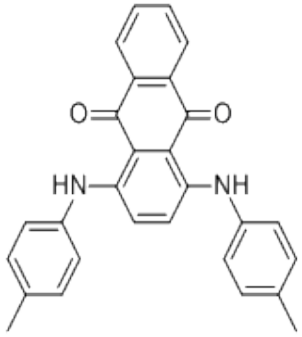

Type of dye	Examples	Structure
Phthalocyanine	Reactive Blue 15	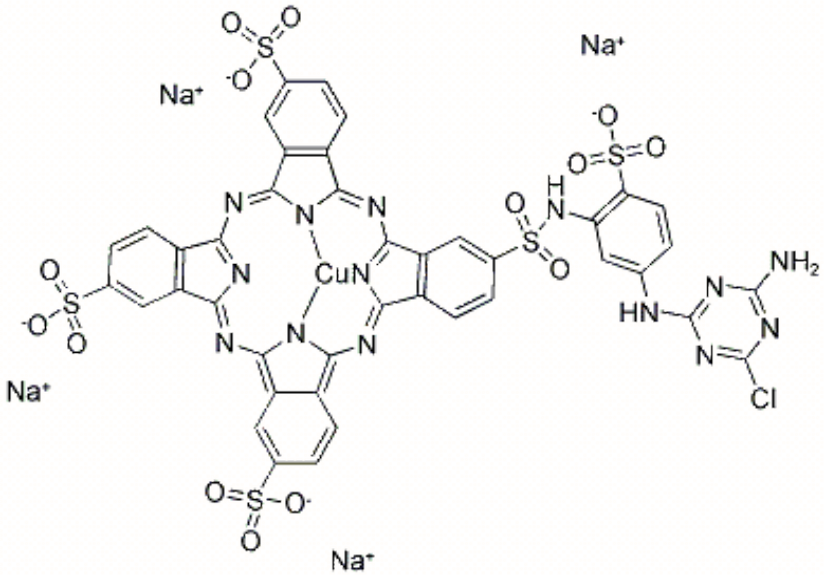

2.2. Basis fundamental principles of photocatalysis

In this section, the typical mechanism of photocatalytic reaction processes is briefly surveyed. Heterogeneous photocatalysis involves a large range of reactions, such as toxic heavy metals removal, water splitting, photoreduction, gaseous effluent purification, anti-cancer therapy, organic synthesis, etc. The fundamental principles of photocatalysis have been established and reported in many literatures.

A semiconductor has a band structure, which is a series of closely spaced energy levels related with covalent bonding between the atoms, forming a crystallite (valance band) and other series of similar levels lying at higher energy relative to the conduction band in the macromolecular crystallite. The energy gap between the electronically filled valence band and the largely vacant conduction band controls the extent of thermal content of the conduction band and its intrinsic state. The band gap is also associated with the wavelengths of light the semiconductor can absorb under solar irradiation. When the semiconductor catalyst is illuminated with photons with an equivalent or greater energy than its band-gap energy, there is absorption of these photons, and the electron from the valance band can be promoted to the conduction band and create an electronic vacancy or hole at the valence band edge. The photogenerated electron usually relaxes thermally to the conduction band edge. The photoexcitation typically produces a balanced amount of electron and holes at the conduction and valence edges, respectively. When the activated electron-hole pairs transfer across the interface, they are capable of reducing and oxidizing a surface-adsorbed substrate and forming a singly oxidized electron donor and a singly reduced electron acceptor.

When the generated hole reaches the surface of semiconductor, it can react with adsorbed

substrate by interfacial electron transfer due to the redox potential of the adsorbed substrate fitting the thermodynamically allowed reaction. Thus, an adsorbed electron donor can be oxidized by transferring an electron to a photogenerated hole on the surface and an adsorbed acceptor can be reduced by accepting an electron from the surface [1]. The chain reactions involved in this process are shown as follows:

Photoexcitation: $Bi_2WO_6 + h\nu \rightarrow e^-_{CB} + h^+_{VB}$ (1)

Oxygen ionosorption: $e^- + O_2 \rightarrow {O_2}^{-\bullet}$ (2)

Ionization of water: $H_2O \rightarrow OH^- + H^+$ (3)

Protonation of superoxides: ${O_2}^{-\bullet} + H^+ \rightarrow HOO^\bullet$ (4)

The hydroperoxyl radical formed in (3) has scavenging property as O_2, which can doubly extend the lifetime of photohole:

$HOO^\bullet + e^- \rightarrow HO_2^-$ (5)

$HOO^- + H^+ \rightarrow H_2O_2$ (6)

Both oxidation and reduction can occur at the surface of photoexcited Bi_2WO_6. Electron-hole pair recombination takes place unless oxygen is available to scavenge the electrons to form superoxides. Its protonated form causes the hydroperoxyl radical to be generated and subsequently, H_2O_2 [3]. The process is given schematically in Figure 2.

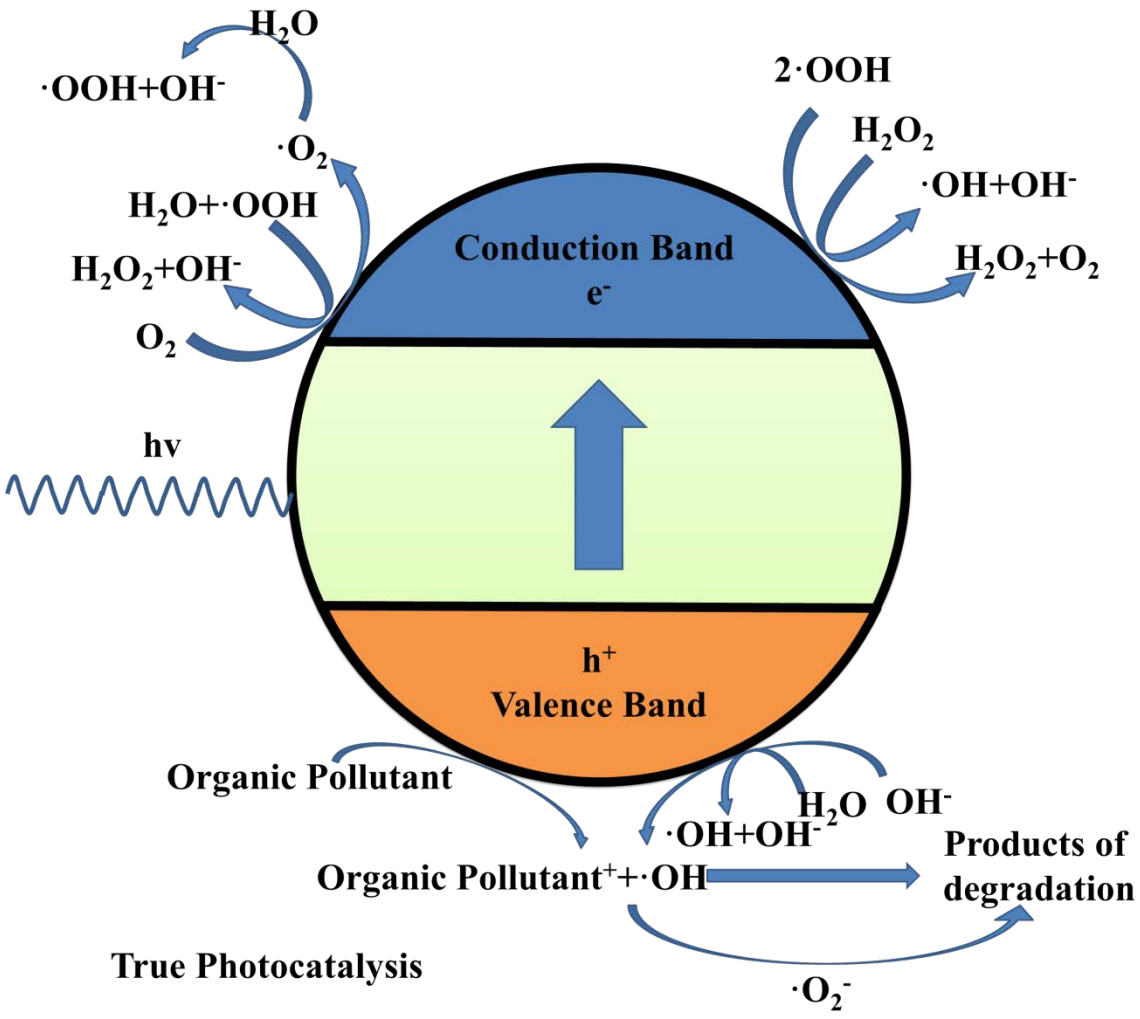

Figure 2 Schematic representations of the possible mechanisms of degrading organic pollutants in the presence of a semiconductor under visible light irradiation.

2.3. Mechanism of Bi_2WO_6-assisted photocatalytic degradation

Bismuth tungstate is a typical n-type direct band gap semiconductor with a band gap of 2.75 eV and has potential applications in solar energy conversion, photocatalyst and electrode materials [4]. In previous studies, it was illustrated that Bi_2WO_6 could act as a stable photocatalyst for the photochemical degradation of organic pollutants under visible light irradiation. Zhang et al. successfully synthesized visible light induced Bi_2WO_6 via a

facile low-temperature combustion synthesis method, and evaluated its photocatalytic activity by decomposition Rhodamine B (RhB) and phenol under visible-light irradiation (λ>420 nm) [5]. Sun et al. used a silica-templated nanocasting method to prepared ordered mesoporous Bi_2WO_6, which was found to have a high activity for the degradation of phenol under visible light illumination [6]. Generally, Bi_2WO_6 has been used as a photocatalyst for generating charge carriers thereby inducing reductive and oxidative processes. The mechanisms involved in Bi_2WO_6 photocatalytic reaction are given as follows:

$$\text{organic pollutant} \xrightarrow[\text{ii) } O_2]{\text{i) } Bi_2WO_6 \\ \text{iii) } h\nu \geq E_g} \text{Intermediate(s)} \longrightarrow CO_2 + H_2O + HA$$

Where HA is the corresponding acid with non-metal substituent.

Many studies have described the mechanistic processes which take place in the photocatalytic decomposition of organic compounds over Bi_2WO_6 surface. Bi_2WO_6 is excited by light irradiation with greater energy than its band gap energy, causing the production of electron-hole pairs in the semiconductor Bi_2WO_6. Thereby redox reactions occur to provide the formation of hydroxyl radicals and superoxide ions that are non-selective strong oxidizing agents that can directly react with organic pollutants, causing their degradation and subsequent mineralization. The organic pollutants can also interact with the photogenerated holes in the valence band of Bi_2WO_6 [7]. The photocatalytic process is described according to the following scheme:

$$Bi_2WO_6 + h\nu \rightarrow e^-_{CB} + h^+_{VB} \quad (7)$$

$$e^- + O_2 \rightarrow {O_2}^{-\bullet} \quad (8)$$

$$\text{Organic pollutants} + O_2/O_2^{-\bullet} \rightarrow \text{products} \quad (9)$$

$$\text{Organic pollutants} + h^+ \rightarrow \text{products} \quad (10)$$

2.4. Trends in improving the photocatalytic activity of Bi_2WO_6

The photocatalytic activity of Bi_2WO_6 is closely associated with its intrinsic properties. Generally, the photoactivity of Bi_2WO_6 is limited by its short photogenerated electron-hole pair lifetimes and the optical absorption visible light region. Due to these limitations, it is necessary to modify Bi_2WO_6 to improve its efficiency and increase its applicability to large-scale applications. To date, two main approaches to modifying Bi_2WO_6 have been identified in the literature. The first method involves doping Bi_2WO_6 with other elements, which can narrow the electronic properties of the host material, and simultaneously improve its optical properties. An alternative method is in the modification of the Bi_2WO_6 surface with other semiconductors or metal nanoparticles, which can enhance the photo-response in the visible light region and improve the charge-transfer efficiency, while simultaneously suppressing electron- hole recombination and promoting enhanced photocatalytic activity in practical applications. Table 2 compares the various Bi_2WO_6-assisted composite photocatalyst performances presented in literature.

Table 2 Comparison of different Bi_2WO_6-assisted composite performances

Types	**Organic pollutants**	**Performances in photoactivity**	**Advances**	**Comments**	**References**
Ag/Bi_2WO_6	Rhodamine B (RhB)	0.5 wt% Ag-loaded Bi_2WO_6 sample exhibited best photocatalytic activity by degradation of 90% of 10 mg/L RhB after being irradiated for 30 minutes	Synergetic effect of metallic Ag and Bi_2WO_6, improving the electron migration efficiency. Optical absorption spectrum red-shifted due to plasmon resonance of Ag nanoparticles	Weak improvement of the photocatalytic activity, unknown effect of operating parameters	[8]
$PtCl_4/ Bi_2WO_6$	Rhodamine B (RhB)	0.8 wt% $PtCl_4/ Bi_2WO_6$ sample exhibited best photocatalytic activity by degradation of 96% of	Improvement of the interfacial charge transfer by high Schottky barrier that restricted the electron hole	High cost, limited optical adsorption spectrum of visible light, unknown	[9]

Types	Organic pollutants	Performances in photoactivity	Advances	Comments	References
		10^{-5} mol/L RhB after 60 minutes irradiation	recombination. Absorption intensity in visible light region enhanced due to charge-transfer transition between metal ions and Bi_2WO_6	stability and effect of operating parameters	
AgBr-Ag-Bi_2WO_6	Procion red MX-5B and Pentachlorophenol	AgBr-Ag-Bi_2WO_6 nanojunction system degraded 42.8 mg/L MX-5B and achieved a removal efficiency of 85% within 60 minutes	AgBr-Ag-Bi_2WO_6 nanojunction system shown to broaden visible light photo-response range. A synergic effect was present between two visible light active components in	High cost, limited optical absorption in the visible light region, complex preparation method	[10]

Types	Organic pollutants	Performances in photoactivity	Advances	Comments	References
			AgBr-Ag-Bi_2WO_6 nanojunction. The vectorial electron transfer was driven by the two step excitation of AgBr and Bi_2WO_6		
Cu^0/ Bi_2WO_6	Phenol	The degradation rate of phenol by Cu^0/ Bi_2WO_6 was three times higher than bare Bi_2WO_6.The removal efficiency reached 80% after 3 hours irradiation.	Combination two different advanced oxidation processes of photocatalysis and Fenton-like used. Doping was by zero valent copper, not copper ions.	Optical absorption spectrum not reported, limited photocatalytic activity	[11]
C_{60}/Bi_2WO_6	Methylene blue	Photocatalytic activities	Conjugative π-system leads	Limited optical	[12]

Types	Organic pollutants	Performances in photoactivity	Advances	Comments	References
	(MB) and Rhodamine B (RhB)	of 1.5 wt% C_{60}/Bi_2WO_6 samples increased degradation by about 5.0 and 1.5 times for MB and RhB after 60 minutes visible light irradiation	to high photogenerated electrons migration efficiency.	absorption in visible light region, high cost, effect of operating parameters unknown.	
Co_3O_4/ Bi_2WO_6	Methylene blue (MB)	The highest efficiency was observed when calcined at 300 °C with 0.2 wt% cobalt content. Co_3O_4/ Bi_2WO_6 samples increased degradation of	Photogenerated charge carrier recombination between the hybrid orbital of Bi 6s and O 2p (VB) to the empty W 5d orbital is inhibited in the composite	Weak improvement of the photocatalytic activity, unknown effect of operating parameters	[13]

Types	Organic pollutants	Performances in photoactivity	Advances	Comments	References
		MB by about 1.1 times in 30of MB in 30 minutes compared to pure Bi_2WO_6	semiconductors. And the optical adsorption of visible light is broad.		
TiO_2/ Bi_2WO_6	Rhodamine B	TiO_2/ Bi_2WO_6 samples increased decomposition of RhB by about 4.6 times in 30 minutes compared to the pure material	Bi_2WO_6 with different morphologies and microstructures could be obtained by adjusting the concentration of the precursor. Small grain size and large surface areas were caused by the incorporation of TiO_2 during synthesis process	Limited optical adsorption in visible light region	[14]

2.5. Influence of operational parameters governing the kinetics

2.5.1 Dosage of photocatalyst

In previous studies, the initial rates of reaction were demonstrated to be proportional to an increase in degradation with the mass of catalyst [15]. However, when the mass of catalyst exceeds a certain value, the reaction rate becomes independent of the dosage of catalyst. Excess photocatalyst particles cause the unfavourable light scattering effect, and diminishes the light penetration into pollutant solution, leading to a decrease in the photocatalytic activity observed. Additionally, for practical applications, the optimum value of mass of catalyst should be determined to avoid excess catalyst dosage and to ensure an efficient absorption of photons during the reaction process.

2.5.2 Initial pollutant concentration

Photocatalytic oxidation of organic pollutants over time relies upon the photonic efficiency, which changes with pollutant concentration. At the high concentration range, the photonic efficiency is reduced and the semiconductor surface becomes saturated, which leads to photocatalyst deactivation [16].

2.5.3 Initial pH value of pollutant effects

When photocatalytic reactions take place on a semiconductor suspension in pollutant solution, the reaction rate is weakly related to the pH value of the pollutant solution, since the pH value of pollutant influences the particle size, surface charge, size of aggregates it forms and band edge positions of photocatalysts. The optimum pH value can enhance the photodegradation efficiency of organic pollutants without influencing the rate equation. Zhang et al. showed that the adsorption and photodegradation of dye pollutants are

pH-dependent, chiefly resulting from the variation of surface charge of catalysts with pH [17].

2.5.4 Temperature effects

Photocatalytic reactions are not sensitive to minor variations in temperature. Most photocatalysis reaction is operated at room temperature without heating from outside, due to the photonic activation. And the true activation energy Et is nil, while the apparent activation energy Ea is very small with the medium temperature range from 20^oC to 80^oC.When the reaction temperature is less than zero, the activity reduces and Ea tends to heat of adsorption of the products. When the reaction temperature is increased above 80^oC, high temperature favors the recombination of charge carriers and desorption process of adsorbed reactant species. So the optimum value of reaction temperature is between 20^oC and 80^oC. This also explains why solar devices requires temperature controller [1, 3].

2.5.5 Quantum yield

The photocatalytic reaction rate relies on the radiation absorption of the catalyst. In a previous study, it was been found that the degradation rate increases with the increase in light intensity during reaction process [18, 19]. Quantum yield is the ratio of the reaction rate in molecules per second (mol/s) to the efficient photonic flux in photons per second (Einstein/s). The theoretical maximum value of quantum yield is equal to 1. The value can range greatly, depending on considerations such as the nature of the catalyst, experimental conditions and the nature of the reaction. The quantum yield can be used to: (1) Compare the photocatalytic activity with different photocatalysts for the same reaction, (2)

Assess the relative feasibility of different reactions, (3) Estimate the energetic yield and the relevant cost [4]. The photocatalyst cannot absorb all the incident radiation because of refraction. There are two predominant factors that affect quantum yield: (1) Light scattering in solid-liquid regime, and (2) Thermal recombination between electrons and holes [1].

2.5.6 Synthesis methods of photocatalyst effects

There are direct connections between the organic pollutant and the surface property of photocatalyst. The surface morphology, particle size and agglomerate size all strongly influence the photocatalyst performance in the photocatalytic oxidation process. Numerous morphology and structures of Bi_2WO_6 have been synthesized by various methods to obtain desirable properties, activity and stability for photocatalytic applications [4]. In Table 3, the morphology and photocatalytic properties of Bi_2WO_6 powders synthesized by various methods are compared.

Table 3 Various morphologies and its photocatalytic properties of prepared Bi_2WO_6

Synthesis methods	**pH value of precursor**	**Morphologies and sizes**	**Performances of photoactivity**	**Comments**	**References**
Co-precipitation method	pH=5	Spherical particles with sizes less than 1 μm	Degradation was monitored over 300 minutes irradiation and removal 80% of initial concentration of 5 mg/L RhB solution was observed. The best half-life time reported was 157 minutes.	Low photocatalytic activity, non-uniform size distribution, large particle size observed	[20]
Ultrasonic-assisted method	Not reported	Thin 2D laminar structure with size of ca. 100 nm	Photocatalytic activities were about 4-6 times higher than material prepared by solid-state method.	Low photocatalytic activity, unknown agglomeration size, high cost	[21]

Synthesis methods	**pH value of precursor**	**Morphologies and sizes**	**Performances of photoactivity**	**Comments**	**References**
Microwave-assisted solvothermal method	pH=9	Large quantity of nanosheets with some nanocrystallites	Complete degradation of 10^{-5} mol/L RhB with approximately 2 hours irradiation	Limited optical absorption visible light region, non-uniform agglomeration size	[22]
Low-temperature combustion method	Not reported	Sphere-shaped morphology with crystallite sizes ranging from 20 nm to 30 nm	Completely degradation of 10^{-4} mol/L RhB within 75 minutes irradiation through 420 nm cut-off filter	High cost, long time calcination time	[23]
Sol-gel method	Not reported	Consist of irregular nanoplates with laminar structure	The removal efficiency reached 97% by degradation of the azo dye 4BS after irradiation for 120 min	High temperature calcinations, non-uniform agglomeration size	[24]

Among all these methods, the hydro-thermal method is most predominantly used to synthesize Bi_2WO_6 micro/nano structures with high photocatalytic activity. The pH of precursor solution has been shown to strongly influence the reaction process and purity of final products, since pH values cause the production of different amounts of H_2WO_4 precipitate, and lead to the production of Bi_2WO_6 with different morphologies [25]. Surfactant is another factor affecting the nucleation and growth of inorganic nanomaterials such as Bi_2WO_6. In recent studies, some groups obtained Bi_2WO_6 with different morphology and structure by tuning pH value and surfactants, to obtain nanoplates, nanoparticles, flower-like, nest-like and nanocage-like superstructure [4]. Table 4 shows the different Bi_2WO_6 morphologies synthesized by hydrothermal method with various pH values of precursor and surfactants used.

Table 4 Bi_2WO_6 morphologies synthesized with various precursor pH values and surfactants

Morpholo-gies	**pH values of precursor**	**Surfactant**	**Sizes**	**Figures**	**References**
Nanoplates	pH=7	Non	Nanoplates approximately ca. 30 nm in size	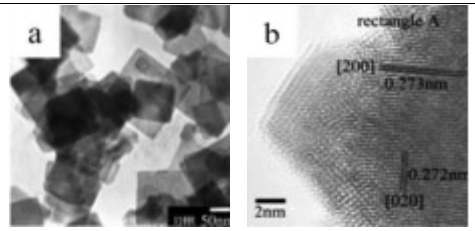	[26]
Nanoparti-cles	pH=7.5	Ethylene glycol	Large quantity of homoge-neous nanoparticles with size of 10 nm	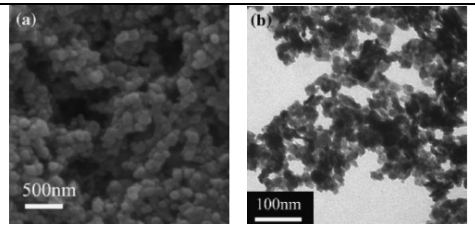	[27]
Flow-er/spere-like superstruc-ture	pH=1	Non	Flower-like spherical super-structures constructed from plenty of nanoplates with single crystal structure	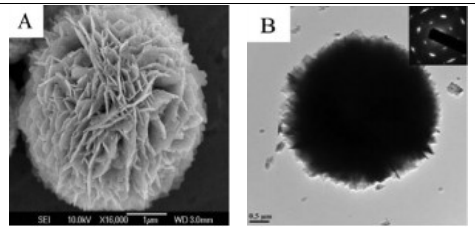	[28]

Morphologies	pH values of precursor	Surfactant	Sizes	Figures	References
Tyre/helix-like superstructure	pH=1	Triblockpoly (ethylene oxide)-block-poly (propylene oxide)-block-poly (ethylene oxide) copolymer (P123)	Nest superstructure constructed with nanobricks with a length about 200 nm and a diameter about 50 nm. The nanobrick subunits were orderly stacked to each other around the center axis of a circle	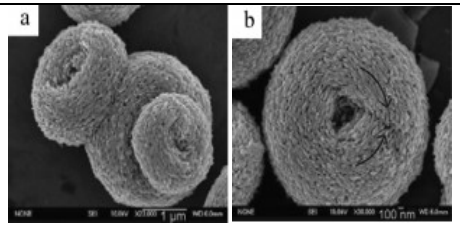	[29]
Nest/ tyre-like superstructure	pH=0-2	Poly (vinyl pyrrolidone) (PVP)/ CTAB	Nest/tyre-like superstructure with an average diameter of about 3-5 μm constructed from plenty of nanosheets with size	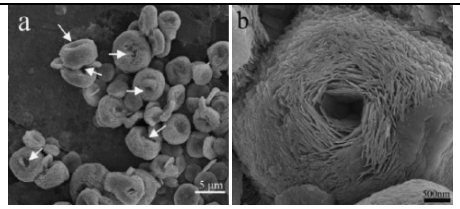	[30]

Morphologies	pH values of precursor	Surfactant	Sizes	Figures	References
			ranging from 16 to 20 nm.		
Nanocage	Not reported	Carbon spheres and ethylene glycol (EG)	Nanocages constructed from small nanoparticles with a size of 50-80 nm. The building blocks of the nanocages grew from small Bi_2WO_6 grains which coated carbon spheres	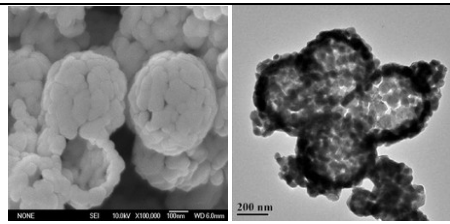	[31]

2.6. Conclusion

The mechanism and photocatalytic applications of Bi_2WO_6 photocatalyst have been described, indicating that Bi_2WO_6 is a visible light driven photocatalytic material that can be considered an exciting and promising photocatalyst of tremendous potential for use in many fields including not only degradation of dyes, but also inactivation of bacteria, fungi, viruses, and spores. However, further investigations are imperative. The high rate of recombination for electron-hole pairs in the bare Bi_2WO_6 material restricts its wider application for photocatalysis. In previous studies, it has been found that there are some drawbacks hindering Bi_2WO_6-assisted photocatalysts lifetimes and limited optical absorptions in the visible light region. To meet the requirements of future practical performance of Bi_2WO_6 photocatalysts, it is necessary to design novel Bi_2WO_6-assisted photocatalysts to further improve photocatalytic efficiencies. Furthermore, the relations among structure, properties and modification of novel visible light driven photocatalytic materials are still to be elucidated, in order to facilitate proper large-scale application of these materials. To address these issues, the synergetic effect between metal and semiconductor components of photocatalysts has been explored in this work. Metallic and ionic Pd species were deposited on Bi_2WO_6 superstructure for the first time, improving the electron migration efficiency through the high Schottky barrier at the interface of the metal and Bi_2WO_6, facilitating charge separation. Metallic and ionic Pd species loaded on the surface of flake-ball Bi_2WO_6 superstructure were synthesized using a template-free hydrothermal method. Rhodamine B (RhB) was chosen as the target pollutant to evaluate the photocatalytic activity of the samples under visible light irradiation.

2.7. References

[1] U. Gayaa, A. Abdullaha, Heterogeneous photocatalytic degradation of organic contaminants over titanium dioxide: A review of fundamentals, progress and problems, Journal of Photochemistry and Photobiology C: Photochemistry Reviews 9 (2008) 1–12.

[2] K. Rajeshwar, M. Osugi, W. Chanmanee, C. Chenthamarakshan, M. Zanoni, P. Kajitvichyanukul, R. Krishnan-Ayer, Heterogeneous photocatalytic treatment of organic dyes in air and aqueous media, Journal of Photochemistry and Photobiology C: Photochemistry Reviews 9 (2008) 171–192.

[3] M. Fox, M. Dulay, Hetrogeneous photocatalysis, Chemical reviews 93 (1993) 341-357.

[4] Y. Tian, G. Hua, W. Xu, N. Li, M. Fang, L. Zhang, Bismuth tungstate nano/microstructures: Controllable morphologies, growth mechanism and photocatalytic properties, Journal of alloys and compounds 509 (2011) 724-730.

[5] Z. Zhang, W. Wang, M. Shang, W. Yin, Low-temperature combustion synthesis of Bi_2WO_6 nanoparticles as a visible-light-driven photocatalyst, Journal of Hazardous Materials 177 (2010) 1013-1018.

[6] S. Sun, W. Wang, J. Xu, L. Wang, Z. Zhang, Highly efficient photocatalytic oxidation of phenol over ordered mesoporous Bi_2WO_6, Applied Catalysis B: Environmental 106 (2011) 559-564.

[7] S. Alfaro, A. Cruz, Synthesis, characterization and visible-light photocatalytic properties of Bi_2WO_6 and $Bi_2W_2O_9$ obtained by co-precipitation method, Applied Catalysis A: General 383 (2010) 128-133.

[8] D. Wang, G. Xue, Y. Zhen, F. Fu, D. Li, Monodispersed Ag nanoparticles loaded on

the surface of spherical Bi_2WO_6 nanoarchitectures with enhanced photocatalytic activities, Journal of Material Chemistry 22 (2012) 4751-4758.

[9] F. Duan, Y. Zheng, M. Chen, Flowerlike $PtCl_4/Bi_2WO_6$ composite photocatalyst with enhanced visible-light-induced photocatalytic activity, Applied Surface Science 257 (2011) 1972-1978.

[10] L. Zhang, K. Wong, Z. Chen, J. C. Yu, J. Zhao, C. Hu, C. Chan, P. Wong, AgBr-Ag-Bi_2WO_6 nanojunction system: A novel and efficient photocatalyst with double visible-light active components, Applied Catalysis A: General 363 (2009) 221-229.

[11] J. Xu, W. Wang, E. Gao, J. Ren, L. Wang, Bi_2WO_6/Cu^0: A novel coupled system with enhanced photocatalytic activity by Fenton-like synergistic effect, Catalysis Communications 12 (2011) 834-838.

[12] F. Duan, Y. Zheng, M. Chen, Synergetic effect of Bi_2WO_6 photocatalyst with C60 and enhanced photoactivity under visible irradiation, Environmental Science and Technology 41 (2007) 6234-6239.

[13] Q. Xiao, J. Zhang, C. Xiao, X. Tan, Photocatalytic degradation of methylene blue over Co_3O_4/Bi_2WO_6 composite under visible light irradiation, Catalysis Communications, 9 (2008) 1247-1253.

[14] M. Shang, W. Wang, L. Zhang, S. Sun, L. Wang, L. Zhou, 3D Bi_2WO_6/TiO_2 hierarchical heterostructure: Controllable synthesis and enhanced visible photocatalytic degradation performances, Journal of Physical Chemistry C, 113 (2009) 14727-14731.

[15] J. Herrmann, Heterogeneous photocatalysis: fundamentals and applications to the removal of various types of aqueous pollutants, Catalysis Today 53 (1999) 115-129.

[16] G.Palmisano, M.Addamo, V. Augugliaro, T.Caronna, A. Paola, E.G. Lopez, V. Lod-

do, G. Marci, L. Palmisano, M. Schiavello, Selectivity of hydroxyl radical in the partial oxidation of aromatic compounds in heterogeneous photocatalysis, Catalysis Today, 122 (2007) 118-127.

[17] L. Zhang, K. Wong, Z. Chen, J. Yu, J. Zhao, C. Hu, C. Chan, P. Wong, AgBr-Ag-Bi_2WO_6 nanojunction system: A novel and efficient photocatalyst with double visible-light active components, Applied Catalysis A: General 363 (2009) 221-229.

[18] M. Qamar, M. Muneer, D. Bahnemann, Heterogeneous photocatalysed degradation of two selected pesticide derivatives, triclopyr and daminozid in aqueous suspensions of titanium dioxide, Journal of Environmental Management 80 (2006) 99-106.

[19] C. Karunakaran, S. Senthilvelan, Photooxidation of aniline on alumina with sunlight and artificial UV light, Catalysis Communications 6 (2005) 159-165.

[20] S. Alfaro, A. Cruz, Synthesis, characterization and visible-light photocatalytic properties of Bi_2WO_6 and $Bi_2W_2O_9$ obtain by co-precipitation method, Applied Catalysis A: General 383(2010) 128-133.

[21] L. Zhou, W. Wang, L. Zhang, Ultrasonic-assisted synthesis of visible-light-induced Bi_2MO_6 (M=W, Mo) photocatalysts, Journal of Molecular Catalysis A: Chemical 268 (2007) 195-200.

[22] L. Wu, J. Bi, Z. Li, X. Wang, X. Fu, Rapid preparation of Bi_2WO_6 photocatalyst with nanosheet morphology via microwave-assisted solvothermal synthesis, Catalysis Today 131 (2008) 15-20.

[23] Z. Zhang, W. Wang, M. Shang, W. Yin, Low-temperature combustion synthesis of Bi_2WO_6 nanoparticles as a visible-light-driven photocatalyst, Journal of Hazardous Materials 177 (2010) 1013-1018.

[24] G. Zhang, F. Lu, M. Li, J. Yang, X. Zhang, B. Huang, Synthesis of nanometer Bi_2WO_6 synthesized by sol-gel method and its visible-light photocatalytic activity for degradation of 4BS, Journal of Physics and Chemistry of Solids 71 (2010) 579-582.

[25] L. Zhang, H. Wang, Z. Chen, P. Wong, J. Liu, Bi_2WO_6 micro/nano-structures: Synthesis, modifications and visible-light-driven photocatalytic applications, Applied Catalysis B: Environmental 106 (2011) 1-13.

[26] C. Zhang, Y. Zhu, Synthesis of square Bi_2WO_6 nanoplates as high-activity visible-light-driven photocatalysts, Chemistry of Materials 17 (2005) 3537-3545

[27] C. Xu, X. Wei, Z. Ren, Y. Wang, G. Xu, G. Shen, G. Han, Solvothermal preparation of Bi_2WO_6 nanocrystals with improved visible light photocatalytic activity, Materials Letters 63 (2009) 2194-2197

[28] L. Zhang, W. Wang, Z. Chen, L. Zhou, H. Xu, W. Zhu, Fabrication of flower-like Bi_2WO_6 superstructures as high performance visible-light driven photocatalysts, Journal of Materials Chemistry 17 (2007) 2526-2532

[29] L. Zhang, W. Wang, L. Zhou, H. Xu, Bi_2WO_6 Nano- And microstructures: Shape control and associated visible-light-driven photocatalytic activities, Small 3 (2007) 1618-1625

[30] Y. Tian, G. Hua, W. Xu, N. Li, M. Fang, L. Zhang, Bismuth tungstate nano/microstructures: Controllable morphologies, growth mechanism and photocatalytic properties, Journal of Alloys and Compounds 509 (2011) 724-730

[31] M. Shang, W. Wang, H. Xu, New Bi_2WO_6 nanocages with high visible-light-driven photocatalytic activities prepared in refluxing EG, Crystal Growth and Design 9 (2009) 991-996

Chapter 3. The synthesis of $PdCl_2/Bi_2WO_6$ and its visible light driven photocatalysts

Abstract

$PdCl_2/Bi_2WO_6$ composite photocatalysts were synthesized by a template-free hydrothermal and isometric impregnation method. The samples were characterized by X-ray diffraction (XRD), scanning electron microscopy (SEM) and X-ray photoelectron spectroscopy (XPS). The results showed that the Pd species loaded on the surface of Bi_2WO_6 was present as $PdCl_2$ and the loading of the $PdCl_2$ species did not affect the crystal structure of pure Bi_2WO_6. Due to synergetic effects between the transition metal and semiconductor component, the loading of $PdCl_2$ species greatly improved the photocatalytic degradation of Rhodamine B under visible light irradiation. The 1 wt% $PdCl_2$ loaded Bi_2WO_6 superstructure sample exhibited the highest activity among the prepared photocatalysts. Furthermore, the removal efficiency of Rhodamine B was found to be influenced by parameters such as catalyst dosage, pollutant concentration and solution pH.

3.1. Introduction

Currently, environmental problems associated with organic pollutants attract tremendous attention, due to their widespread and severe threats to sustainable development. To address this problem, heterogeneous photocatalysis presents a good option for remediation in environmental applications, such as for heavy toxic metal ions removal [1], industrial textile wastewater treatment [2], gaseous effluents purification [3], photocatalytic polymers degradation [4], and microbial cell sterilization [5]. TiO_2 semiconductor is widely used because it possesses a relatively high photocatalytic efficiency to decompose organics. However, TiO_2 can only be activated under ultraviolet radiation, which accounts for about 4% of the incoming solar spectrum, while visible light which occupies more than 43% of the total solar radiation cannot be utilized by TiO_2. To optimize the use of solar energy, visible light driven (VLD) photocatalytic materials have been considered in recent years. There are two main approaches to prepare VLD photocatalysts. One is modifying the TiO_2 by doping with ions, transition metal or semiconductor coupling. Many studies focused on the second approach, which promotes to develop novel VLD photocatalysts such as $BiVO_4$, CdS, $CaIn_2O_4$, $NaTaO_3$ and so on.

Recently, Bi_2WO_6 has been demonstrated to exhibit an excellent photocatalytic activity and solar energy utilization for the degradation of organic compounds under visible light irradiation [6]. In the previous studies, Bi_2WO_6 was mainly synthesized via the solid-state method. Kudo et al. [7] reported Bi_2WO_6 to have a visible-light-induced photoactivity for water splitting for O_2 and H_2 evolution. Zou's work [8] showed that Bi_2WO_6 has a relatively high photocatalytic activity with visible light absorption ability to mineralize $CHCl_3$ and CH_3CHO pollutants. Both Kudo et al. [7] and Zou et al [8] used the solid state

method to prepare their Bi_2WO_6 particles. However, the solid state method results in Bi_2WO_6 with large crystal particle sizes and small surface area, limiting the photocatalytic activity, since this is dependent on the size, structure and morphology of photocatalyst. Our previous investigation of effect of synthesis method on nanostructure and surface properties indicated that the powders prepared by hydrothermal method were superior to those prepared using the solid state method and coprecipitation, respectively. Despite this, the high rate of recombination for electron-hole pairs in the bare material restricts its large-scale application for photocatalysis [9]. To eliminate this shortcoming, some researchers have proposed the modification of Bi_2WO_6 with other semiconductors or metal such as $PtCl_4$ [10], TiO_2 [11], Cu [12], Ag [13], Co_3O_4 [14], C_{60} [15], and AgBr-Ag-Bi_2WO_6 nanojunction [16]. Metals-loaded Bi_2WO_6 has been shown to improve the electron migration efficiency through the high Schottky barrier at the interface of the metal and Bi_2WO_6, so that the charge separation is facilitated [17]. Transition metals such as Pt, and Pd have very efficient photocatalytic properties for many significant reactions. Pt/TiO_2 and Pd/TiO_2 systems were proposed by Colmenares et al. [18], and were shown to exhibit better photocatalytic activity for hydrogen production with thermal treatment at 850^{o}C due to electron transfer from titania to the metal through a support- interaction effect. In our research, the carrier-Bi_2WO_6 was prepared by hydrothermal method.$PdCl_2$-deposition onto Bi_2WO_6 at different loading contents was then employed to enhance its photocatalytic activity of degradation of Rhodamine B under visible light irradiation. It was found that $PdCl_2/Bi_2WO_6$ has higher photocatalytic activity than pure Bi_2WO_6, due to the Pd metal avoiding the quick rate of recombination for electron-hole pairs.

3.2. Experimental

3.2.1 Catalyst preparation

The Bi_2WO_6 samples were synthesized by a template-free hydrothermal method. All chemicals were reagent grade and used without further purification. In a typical synthesis, 0.98 g of $Bi(NO)_3 \cdot 5H_2O$ (ACS reagent grade, 98%) was dissolved in 40 mL acetic acid and 0.33 g of $Na_2WO_4 \cdot 2H_2O$ (purum grade, 99%) was dissolved in 20 mL deionized water, respectively. Then Na_2WO_4 solution was added dropwise to the $Bi(NO)_3$ solution under magnetic stirring for 30 minutes. The pH value of the suspension was adjusted to 1 using hydrochloric acid solution (0.5 mol/L, Sigma-Aldrich). The suspension was sealed in a Teflon-lined stainless steel autoclave at 60% of its maximum volume and heated 180^{o}C for 20 hours, and then gradually cooled to room temperature. The resulting sample was filtered and washed twice with deionized water and dried in an oven at 80^{o}C for 2 hours.

The $PdCl_2$ loaded Bi_2WO_6 sample was prepared by an isometric impregnation method. A calculated concentration of $PdCl_2$ solution was added to 0.5 g Bi_2WO_6 to obtain different mass percents within the range of 0.5-2.0 wt%. The suspension was stirred using a glass rod and dried in ambient air. The resulting powder was collected and heated in the oven at 80^{o}C for 2 hours.

3.2.2 Characterization

X-ray diffraction (XRD) patterns of all prepared powders were collected using Rigaku Ultima IV XRD with Cu K(α) source operating at 40 kV and 40 mA over the range of $2\theta = 10^o$ to 80^o. The wavelength of X-ray radiation used was 0.15418 nm.

X-ray photoelectron spectra (XPS) data were collected on a Kratos Axis Ultra with monochromatized Al Kα radiation at 14 kV and 140 W. The binding energies were referred to the C 1s hydrocarbon peak at 283 eV.

The scanning electron microscope (SEM) images were obtained on a JEOL JSM-7500F field emission scanning microscope.

The ultraviolet visible (UV-vis) light diffuse reflectance spectra of the samples were recorded on a UV-vis spectrophotometer (Puxi, UV1901).

3.2.3 Photocatalytic degradation experiments

The photocatalytic activities of all samples were evaluated by degradation of Rhodamine B (RhB) (dye content, 95%) in an aqueous solution under visible-light irradiation using a 300 W tungsten halide lamp filtered through a 420 nm UV cut-off filter (Kenko Zeta, transmittance>90%). In order to avoid the effect of thermal catalytic reaction, the temperature of the reactor was controlled around $20^{o}C\pm2$ by a cooling/heating recirculating water cooling jacket. The given amounts of $PdCl_2/Bi_2WO_6$ photocatalysts were added to a 500 mL beaker containing 100 mL Rhodamine B aqueous solution. The pH value of the mixture was adjusted by either sodium hydroxide (0.5 mol/L, Sigma-Aldrich) or hydrochloric acid solution (0.5 mol/L, Sigma-Aldrich). Prior to illumination, the suspension was magnetically stirred for 30 minutes in the dark to achieve adsorption/desorption equilibrium between the photocatalyst and the dye. The suspension was then exposed to visible light irradiation under constant magnetic stirring. At given irradiation time intervals (10 minutes), 1mL of suspension was collected and centrifuged to separate the photocatalysts (12000 rpm, 3 minutes). The reaction solution was measured by a Genysys 10-UV spectrophotometer (Geneq Lnc.) with the peak adsorption at 552 nm. A calibra-

tion curve was used to determine the Rhodamine B concentration from the absorbance. The photocatalytic degradation efficiency was calculated by the following equation:

$$\text{Degradation efficiency}(\%) = \frac{C_0 - C}{C_0} * 100\% \quad (1)$$

where C_0 is the initial concentration of Rhodamine B (mg/L) and C is the concentration (mg/L) at any time t (min) during the degradation.

3.3. Results and discussion

3.3.1 XRD and XPS analysis

The XRD pattern of pure Bi_2WO_6 and $PdCl_2$/ Bi_2WO_6 powders prepared by hydrothermal method are shown in Figure 3. All the diffraction peaks in the XRD patterns of the samples can be well indexed to the standard data for Bi_2WO_6 (DB Card No.: 01-075-5628). The modification of this material by $PdCl_2$ species did not cause any change in the peak positions and shapes in the composite material, compared to the pattern of the pure Bi_2WO_6. From the XRD data, it was concluded that $PdCl_2$ modified Bi_2WO_6 through the hydrothermal route did not affect the crystal structure of the Bi_2WO_6 photocatalyst. Moreover, the absence of a peak corresponding to Pd can be attributed to low metal ion amounts of Pd species introduced as well as high dispersion of metal ion deposits on the Bi_2WO_6 nanoparticles, which implied that Pd did not replace the atoms in the crystal lattice of Bi_2WO_6, but may have resided on the surface of Bi_2WO_6.

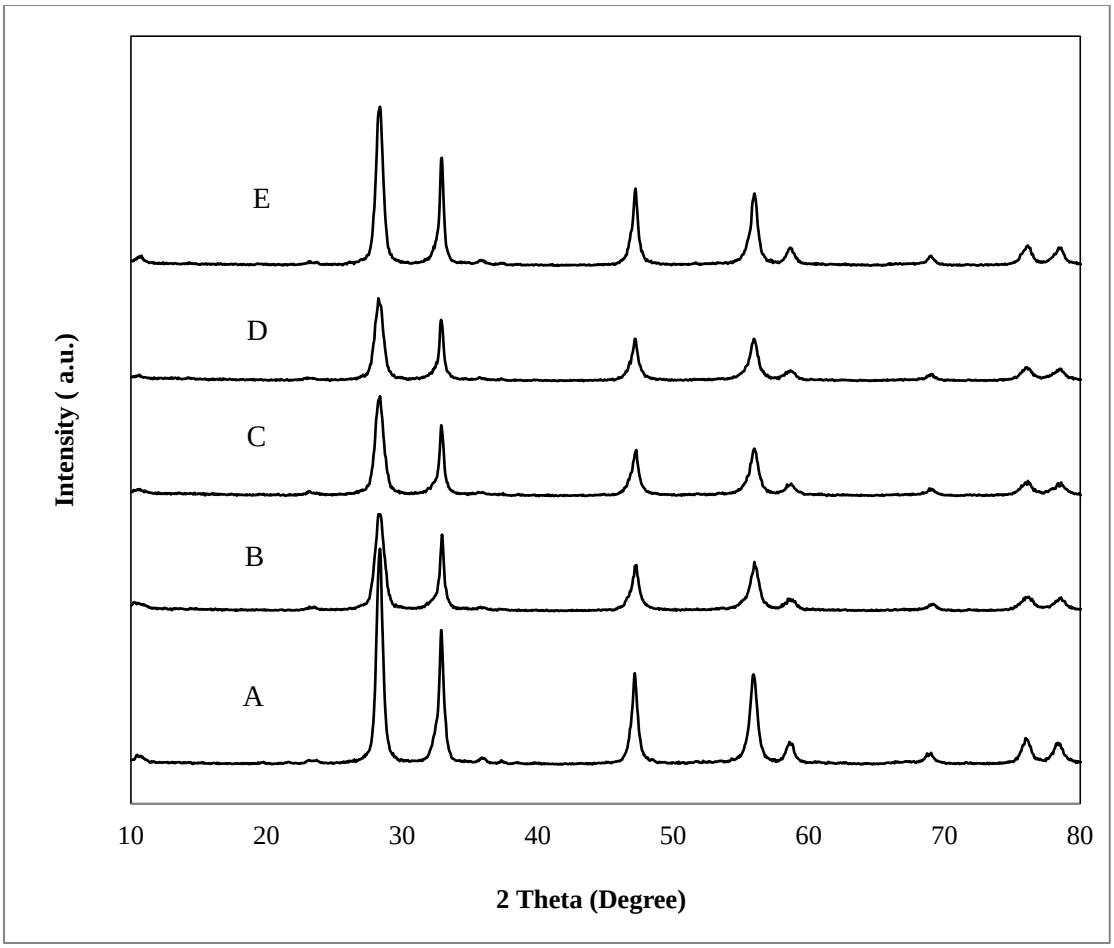

Figure 3 XRD patterns of pure Bi_2WO_6 (A) and Bi_2WO_6 loaded with various contents of $PdCl_2$ species 0.5 wt% (B), 1 wt% (C), 1.5 wt% (D) and 2 wt% (E)

In order to investigate the chemical state of the elements in $PdCl_2/Bi_2WO_6$ with different loading contents, XPS patterns were obtained by scanning the Bi 4f, W 4f, O 1s, Pd 3s and Cl 2p levels. All samples showed similar results to the 1 wt% $PdCl_2/Bi_2WO_6$, as depicted in Figure 4. The presence and state of the Pd species (Pd^0, Pd^{2+} and Pd^{4+}) was mainly revealed by XPS. As shown in Figure 4A, the binding energy of the Pd $3d_{5/2}$ and Pd $3d_{3/2}$ orbital were observed around 335.8 eV and 341.1 eV respectively, which have been found in the literature to be the Pd^{2+} species on the photocatalytic surface [19, 20]. Furthermore, the pure Pd 3d orbit showed two peaks at 335 eV and 340 eV, respectively.

The binding energy for Pd for $PdCl_2/Bi_2WO_6$ was higher than that of pure $PdCl_2$ indicating that a higher electronic density of Pd^{2+} in $PdCl_2/Bi_2WO_6$ was present than that in the pure $PdCl_2$. The Cl 2p peaks appeared at 198.2 eV and 198.9 eV (shown in Figure 4B), indicating the presence of Cl^- as a counterion [10, 21]. Due to the atomic concentration ratio of Pd (1.66%) and Cl (3.30%), we assumed that the Pd species loaded on the surface of Bi_2WO_6 was $PdCl_2$. As shown in Figure 4C, the binding energy for Bi $4f_{7/2}$ and Bi $4f_{5/2}$ were observed at 163.1 eV and 157.6 eV, revealing a trivalent oxidation state of bismuth. The W 4f orbital peaks at 36.1 eV and 34 eV (shown in Figure 4D) indicated a W^{6+} oxidation state for tungsten. As shown in Figure 4e, the O 1s XPS spectrum peak at 529 eV demonstrated that the oxygen species were lattice oxygen [22].

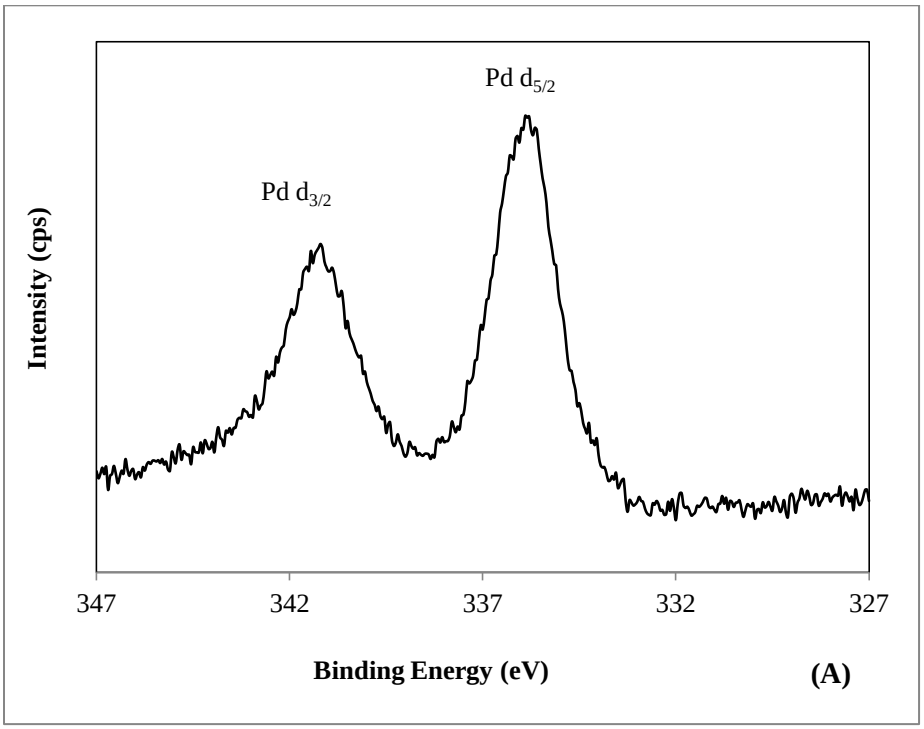

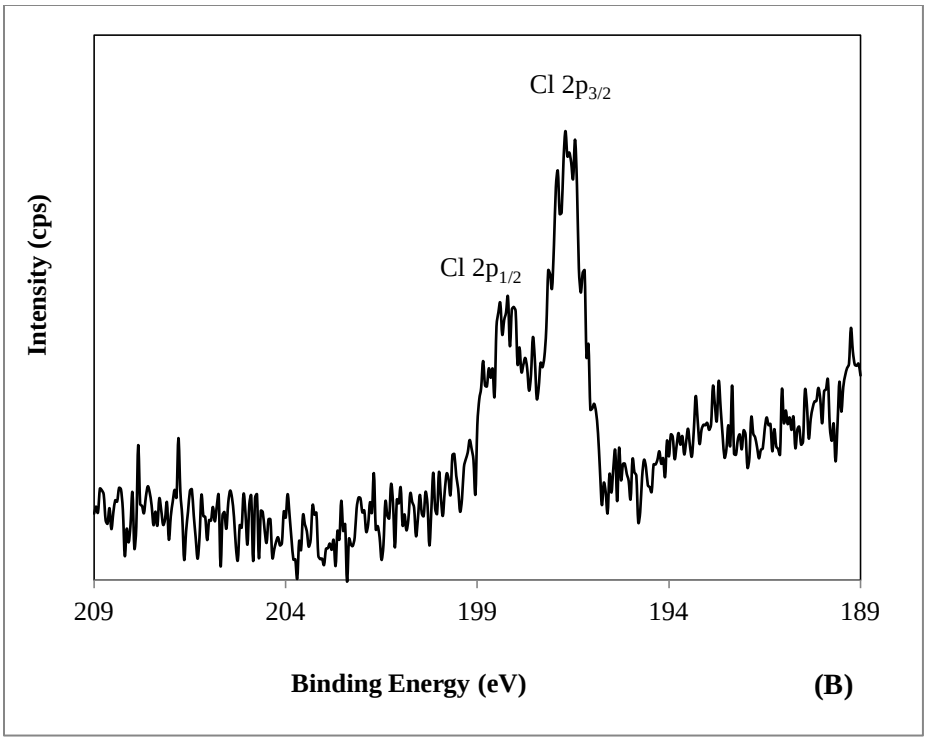
Cl 2p3/2
Cl 2p1/2
Intensity (cps)
209
204
199
194
189
Binding Energy (eV)
(B)

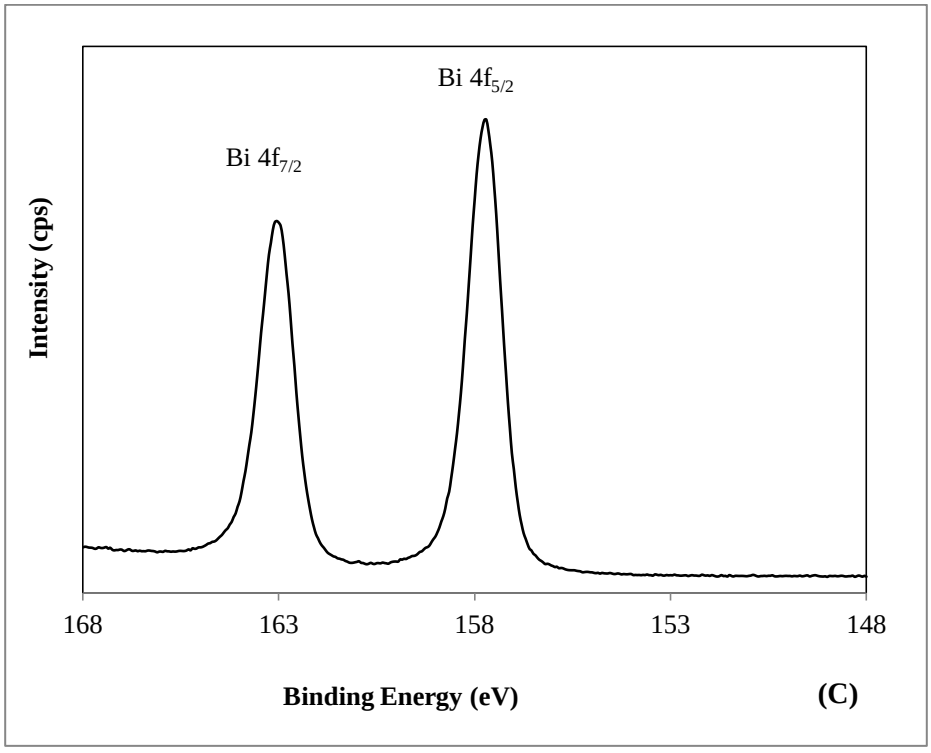
Bi 4f5/2
Bi 4f7/2
Intensity (cps)
168
163
158
153
148
Binding Energy (eV)
(C)

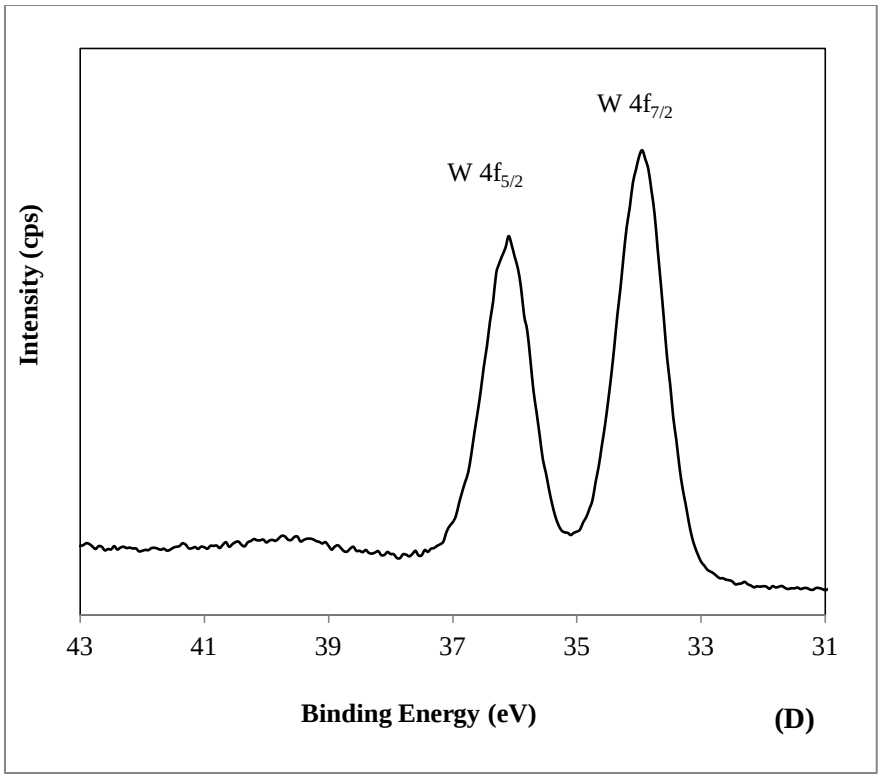

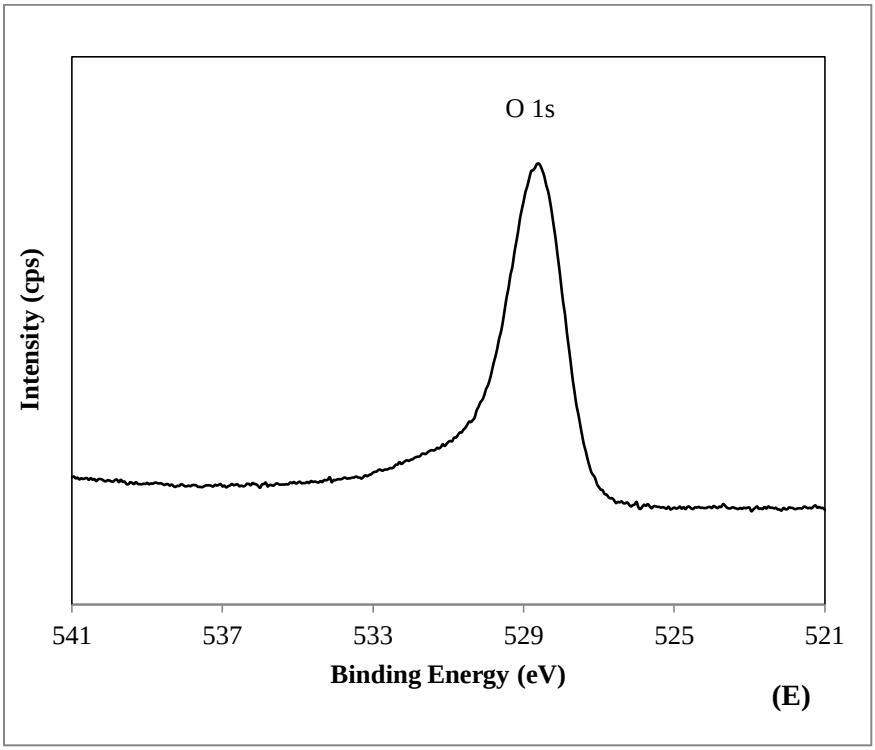

Figure 4 XPS spectra of Pd 3d (A), Cl 2p (B), Bi 4f (C), W 4f (D) and O 1s (E) in $PdCl_2/Bi_2WO_6$ composite (1 wt% $PdCl_2$ loading)

3.3.2 SEM observation

Because of the dependence of light absorption and reaction efficiency on the catalyst surface structure and morphology, the surface structure has an influence on the photocatalytic reaction. Consequently, the morphology of Bi_2WO_6 sample was analyzed by SEM to show the particle size, structure and shape. The samples for SEM imaging were prepared by a simple hydrothermal method without any surfactant. Figure 5 showed the SEM images of pure Bi_2WO_6 samples and 1 wt% $PdCl_2/Bi_2WO_6$ composite photocatalyst. As observed in Figure 5a, the morphology of the pure Bi_2WO_6 consisted of uniform spherical microparticles with the diameter approximately 7 μm. Additionally, high magnification SEM image observed in Figure 5b clearly showed that the flake-ball superstructure of Bi_2WO_6 was constructed from plenty of two-dimensional nanoflakes, which were closed packed and formed a hierarchical structure. The SEM images of 1 wt% $PdCl_2/Bi_2WO_6$ composite photocatalyst (shown in Figure 5c.) also had a uniform size distribution and the hierarchical constructure, which indicated the morphology and constructure of Bi_2WO_6 did not change during the impregnation process.

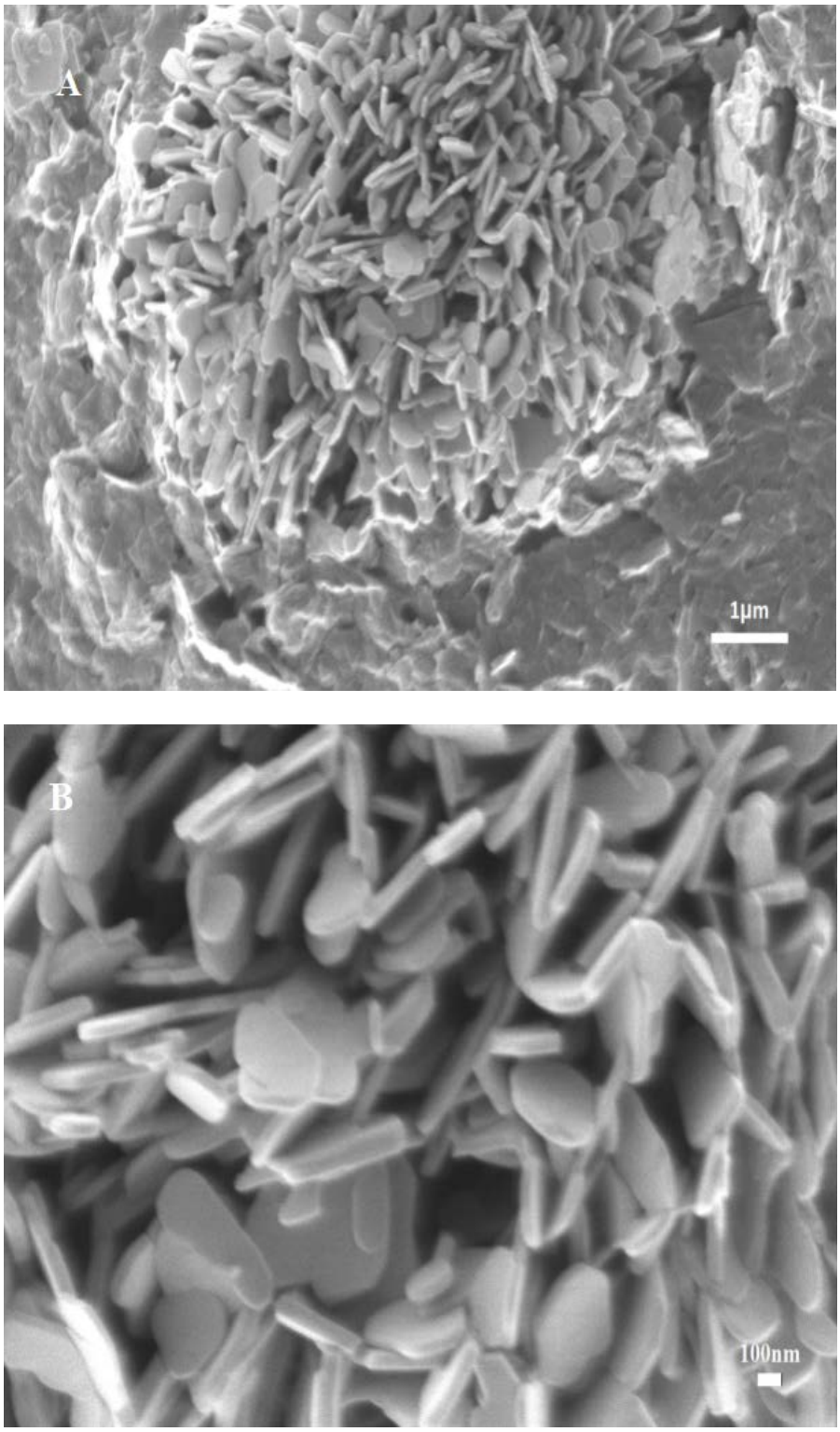
A
1μm
B
100nm

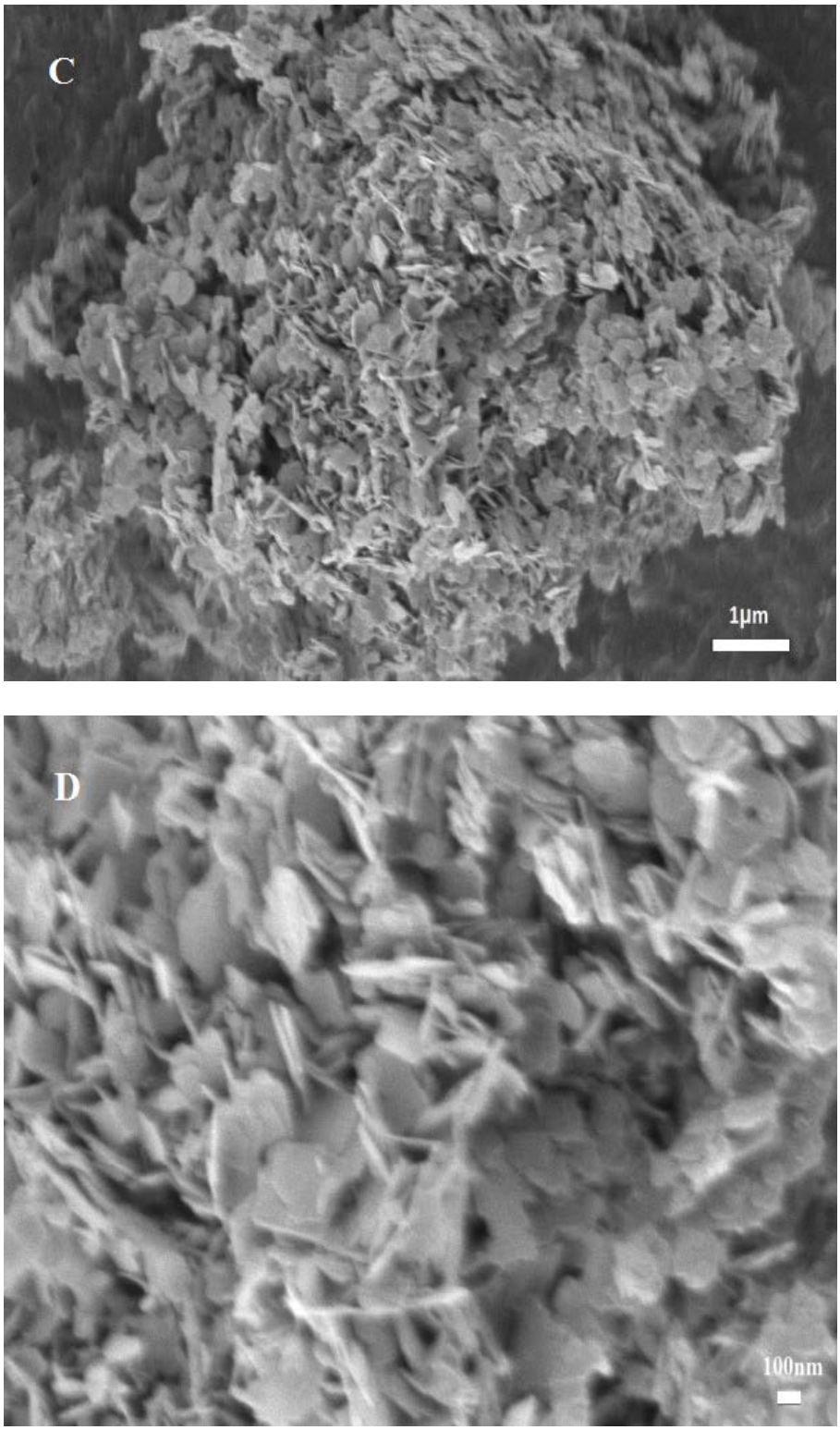

Figure 5 SEM images of pure Bi_2WO_6 (A) and (B), 1 wt% $PdCl_2/Bi_2WO_6$ composite (C) and (D)

The pH value of the precursor solution has very important effect influencing the morphology and purity of the host Bi_2WO_6. The host Bi_2WO_6 prepared with different pH values and template can formulate different morphology, such as flake-ball superstructure (pH=1, without template), Helix/tyre superstructure (pH=1, with P123/CTAB/PVP/IL), disintegrated flower-like superstructure (pH=2.5), or plate structure (pH=7, without template) [23]. In the previous research, it was identified that the low pH value (pH=7） facilitated the formation of Bi_2WO_6. In this experiment, we prepared the flake-ball superstructure under the condition (pH=1 and no template). Under the hydro-thermal process, the relevant chemical reactions for formulation of Bi_2WO_6 can be illustrated as below [24].

$$WO_4^{2-} + 2H^+ \rightarrow H_2WO_4 \downarrow \quad (1)$$

$$Bi(NO_3)_3 + H_2O \leftrightarrow BiONO_3 + 2H^+ + 2NO_3^- \quad (2)$$

$$BiONO_3 + H_2O \leftrightarrow Bi_2O_2(OH)NO_3 + H^+ + NO_3^- \quad (3)$$

$$Bi_2O_2(OH)NO_3 + H_2WO_4 \rightarrow Bi_2WO_6 + H^+ + NO_3^- + H_2O \quad (4)$$

The mechanism for the growing steps of flake-ball particles can be divided as following (Figure 6). Nanoparticles were obtained in the white precipitate which was formed by mixing $Bi(NO)_3$ solution and Na_2WO_4 aqueous solution. The spherical microparticles were formed upon the self-aggregation of nanoparticles, due their thermodynamic stability. Further reaction caused the formulation of 2D nanoflake structure through the dissolution-recrystallization process (Ostwald ripening), accompanied with the microparticle growth. With the increasing reaction time, the flake-ball structure was formed by a nanoflake-organization process, which led to a simple array of nanoflakes generated as spherical flake-like superstructures [6, 23].

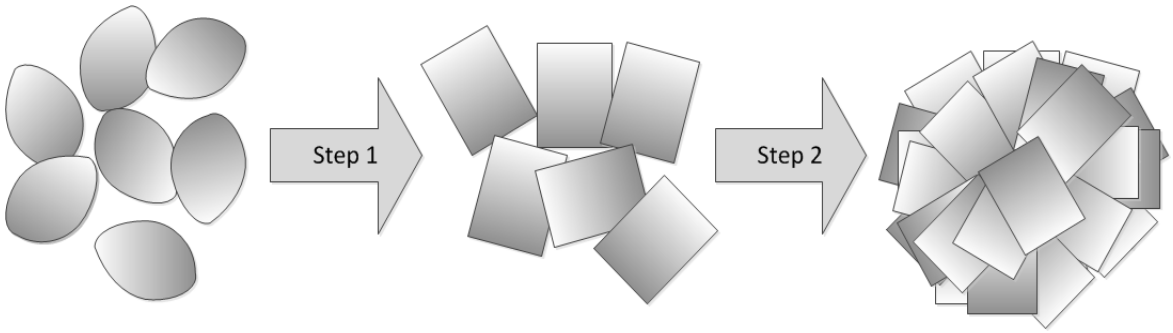

Figure 6 Growth process of flake-ball superstructure of Bi_2WO_6 [13]

3.3.3 UV-vis diffuse absorption spectra

The UV-vis diffuse reflectance spectra were used to measure the optical absorption property of pure Bi_2WO_6 and the $PdCl_2/Bi_2WO_6$ composite photocatalysts. According to the typical diffuse reflection spectrum of the pure Bi_2WO_6 in the Figure 7, the flake-ball Bi_2WO_6 superstructure presented the photo-absorption properties from the UV light region to the visible light absorption at approximately 460 nm. Corresponding with its absorption spectrum, the color of the sample was light yellow. The steep shape of the spectrum showed that the visible light absorption was not caused by the transition from the impurity level but caused by the band gap transition [25]. The considerable reason for visible light absorption of Bi_2WO_6 was due to the transition from the hybrid orbital of O 2p and Bi 6s to the W 5d orbital. For the $PdCl_2$ loaded composite, the absorption spectrum red-shifted, and the edge were found approximately at 510 nm. The reason for the observed red-shift could be the charge-transfer transition between the metal ions and the Bi_2WO_6 conduction or valance band [10]. The band gap energy can be calculated by the formula as below [26]:

$$\lambda = 1240/E_g \quad (1)$$

where λ, E_g are the wavelength (nm) and the band gap energy (eV).

According to this formula, the band gap energy of pure Bi_2WO_6 was 2.69 eV, which was close to the reported value [6, 25, and 27]. The band gap energy of $PdCl_2/Bi_2WO_6$ composite was 2.43 eV, representing a decrease in the band gap and improved visible light absorption. The visible light absorption of the composite photocatalysts was significantly improved by loading $PdCl_2$ and the absorption edge shifted to the visible light range.

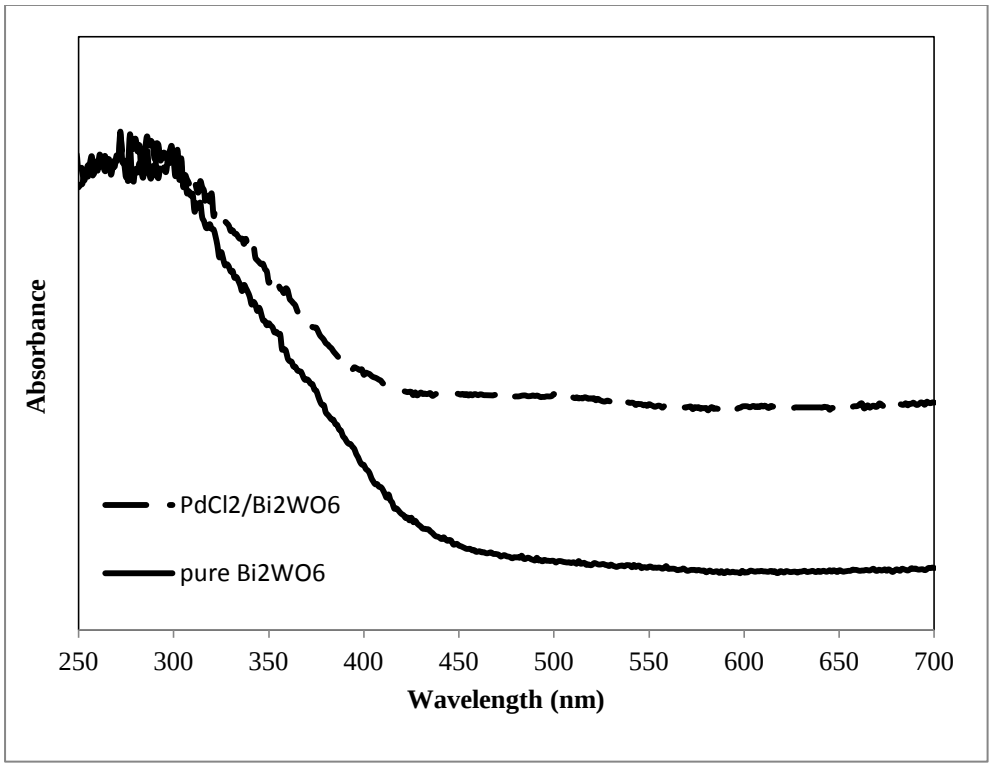

Figure 7 UV-vis diffuse absorption spectra of pure Bi_2WO_6 and the $PdCl_2/Bi_2WO_6$ composite (1wt% $PdCl_2$ loading)

3.3.4 Effect of $PdCl_2$ loading

The photocatalytic activity was evaluated by the degradation of Rhodamine B under visible light irradiation. Compared to pure Bi_2WO_6, the $PdCl_2/Bi_2WO_6$ composite samples with different $PdCl_2$ loadings exhibited excellent photocatalytic activities. In this study, no obvious degradation was observed during the blank test and dark test, indicating that

the dye was stable under visible light irradiation, and adsorption of RhB had a negligible impact on reaction after the adsorption-desorption equilibrium. The results in Figure 8 and Figure 9 showed that the different $PdCl_2$ loadings on Bi_2WO_6 surface quantified by the removal of RhB from solution under visible light irradiation. The removal efficiency of 1 wt% $PdCl_2/Bi_2WO_6$ composite reached 94.09% within one hour degradation, and the removal efficiencies of 0.5 wt%, 1.5 wt% and 2 wt% were 65.18%, 89.45% and 85.60%, respectively. Figure 9 clear shows an optimum value of 1 wt% Pd loading. The photodegradation efficiency increased with the increase in the $PdCl_2$ loadings until the optimum value and decreased with higher $PdCl_2$ loadings. The increasing photocatalytic activity may be explained by the possible production a new energy level located in the band gap of Bi_2WO_6. In this state, electron-hole pairs can be produced by a photon with a higher wavelength than the band gap energy. Electron-hole separation was also in effect for $PdCl_2/Bi_2WO_6$, which led to an increase of photocatalytic activity. The lower band gap and higher crystallinity played the significant role for increasing photoactivity [28]. When the $PdCl_2$ loadings on the surface of Bi_2WO_6 exceeded the optimum amount, the active sites on the Bi_2WO_6 surface were thought to be covered, reducing the efficiency of charge separation. Therefore, a balance should be considered between the creation of active trapping sites and the restriction of electron-hole pairs recombination, and a lower capacity for separation of interfacial charge transfer caused by fewer trapped parts [10].

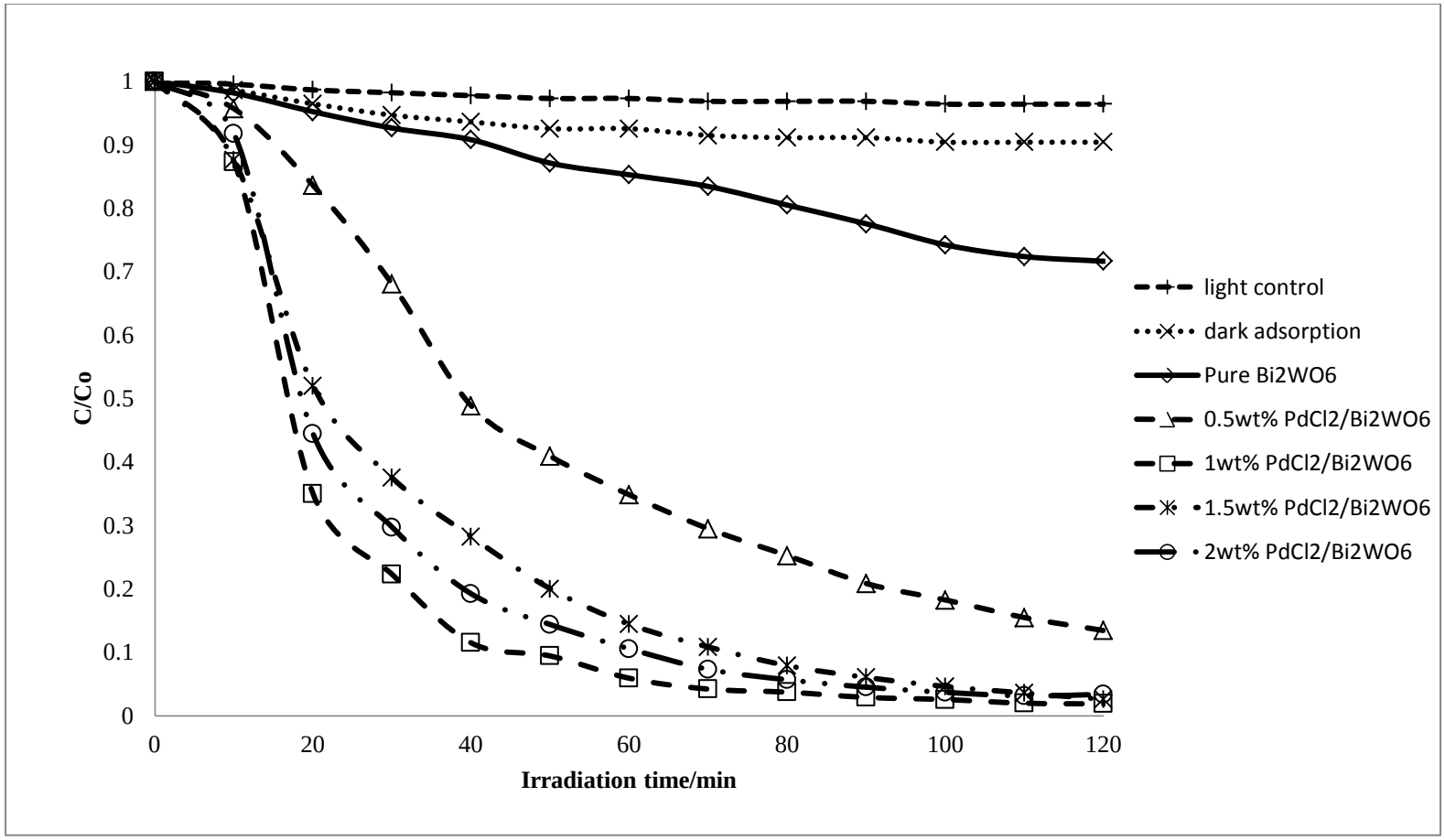

Figure 8 Normalized RhB concentration during degradation with different photocatalysts: (a) light control (without photocatalyst) (b) dark adsorption (without lamp) (c) pure Bi_2WO_6 (d) 0.5 wt% $PdCl_2/Bi_2WO_6$ (e) 1 wt% $PdCl_2/Bi_2WO_6$ (f) 1.5 wt% $PdCl_2/Bi_2WO_6$ (g) 2 wt% $PdCl_2/Bi_2WO_6$

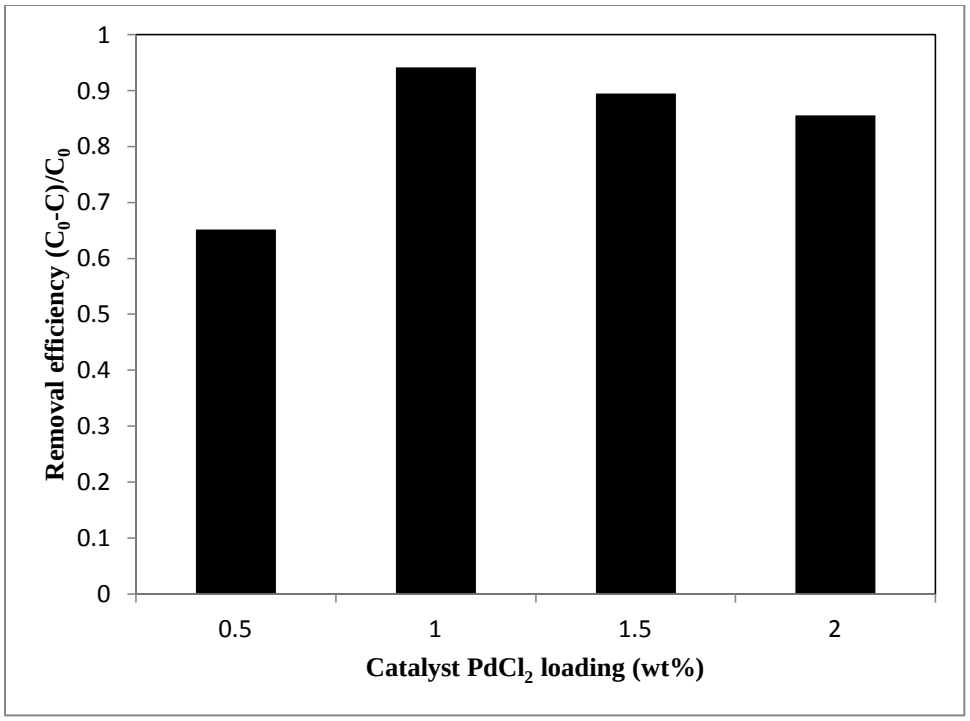

Figure 9 Removal efficiency of different samples within one hour degradation: (a) 0.5 wt% $PdCl_2/Bi_2WO_6$ (b) 1 wt% $PdCl_2/Bi_2WO_6$ (c) 1.5 wt% $PdCl_2/Bi_2WO_6$ (d) 2 wt% $PdCl_2/Bi_2WO_6$

3.3.5 Effect of catalyst dosage

The effect of different dosages of $PdCl_2$/ Bi_2WO_6 on the photocatalytic degradation of RhB was studied and is shown in Figure 10 and Figure 11. The concentration of RhB was kept at 100 mg/L, and the dosage of $PdCl_2/Bi_2WO_6$ was varied from 0.5 g/L to 6 g/L. The removal efficiency increased with the increase of catalyst dosage from 0.5 g/L to 4 g/L. When the catalyst dosage was 4 g/L, the removal efficiency reached 97.5% after one hour of visible light irradiation. A decrease was observed when the catalyst dosages increase from 4 g/L to 6 g/L. The increase dosages of $PdCl_2/Bi_2WO_6$ photocatalyst extended more active surface area which corresponded to the increasing of active sites. Therefore more

active sites were available to produce more hydroxyl radicals and consequently removed pollutants more efficiently. Excessively increasing this dosage induced the increasing of light scattering and decreasing of light penetration which eventually led to the decrease of photocatalytic degradation of pollutants [29].

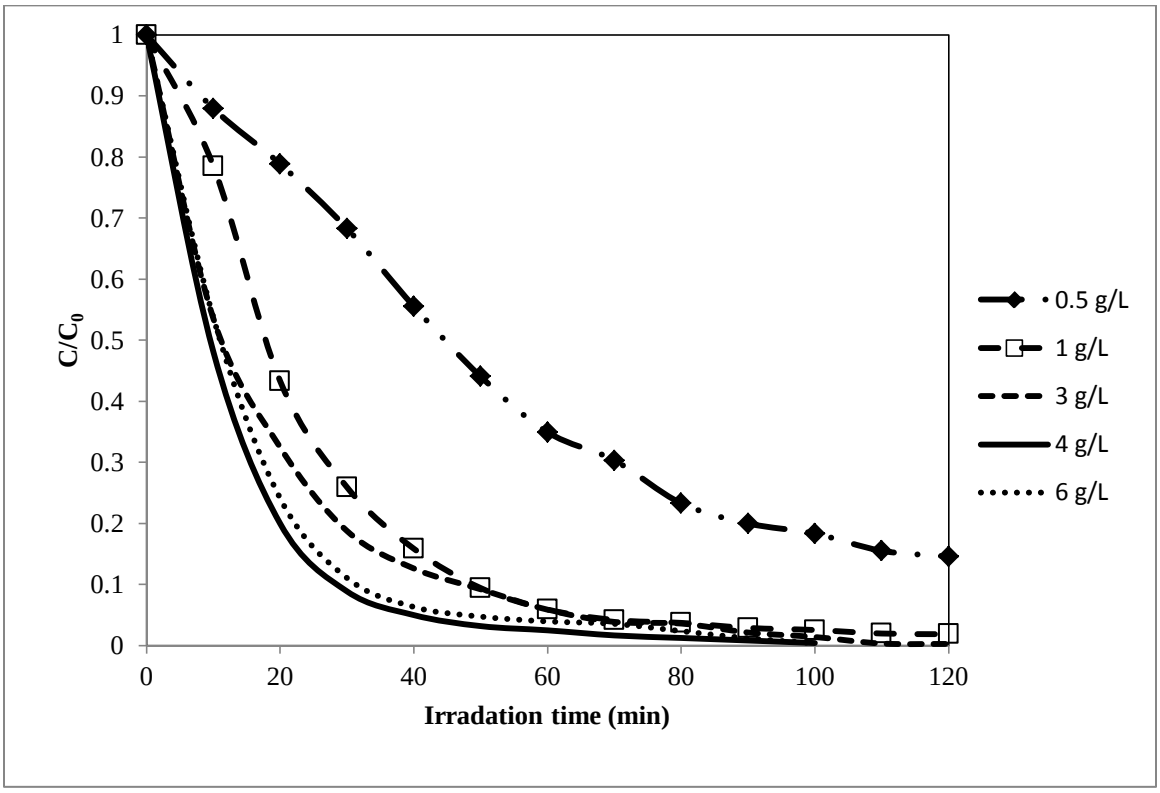

Figure 10 Effect of various dosages of 1 wt% $PdCl_2/Bi_2WO_6$ composite on RhB degradation

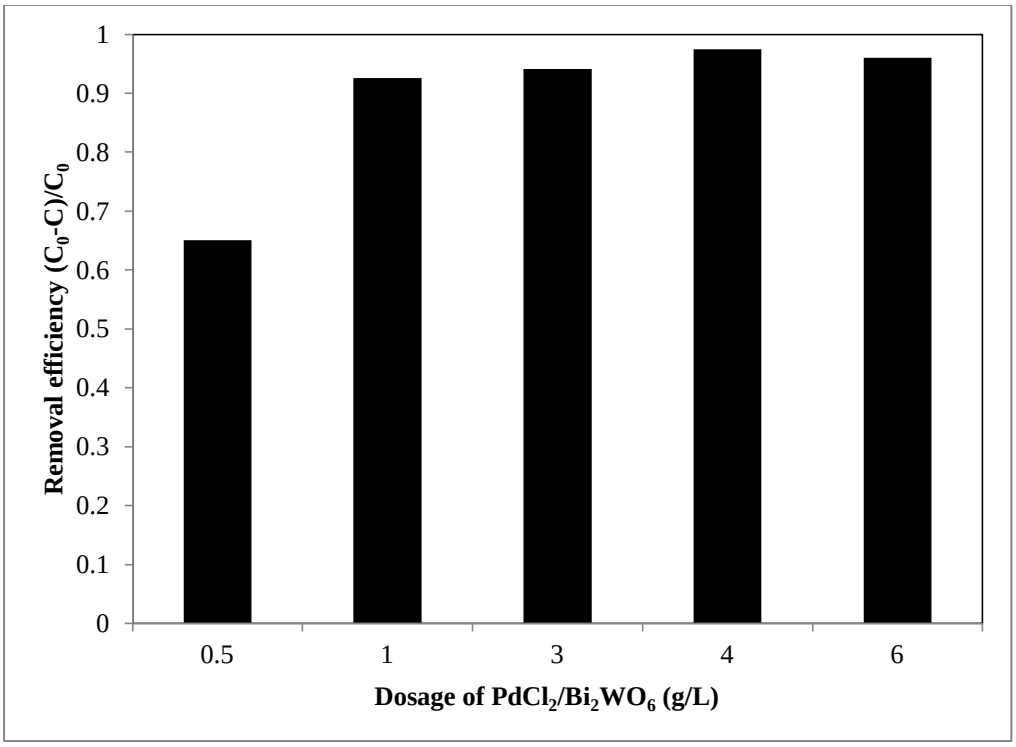

Figure 11 Removal efficiencies of various dosages of 1 wt% $PdCl_2/Bi_2WO_6$ composite within one hour degradation

3.3.6 Effect of initial pH value of RhB

The influences of pH value of RhB solution on the removal efficiency were investigated and the results are displayed in Figure 12 and Figure 13. The removal efficiency increased with an increase of initial pH value from 3 to 4 and decreased when the initial pH value increased from 4 to 10. Previous research indicated that pH value influenced the adsorption and degradation of dye pollutants, which caused the variation of surface charge of photocatalyst with pH value of pollutant solution. A variation in pH value from 3 to 10 influenced the degradation of RhB in aqueous $PdCl_2/Bi_2WO_6$ dispersion. The highest removal efficiency was achieved at pH 4. The prevailing pH of the solutions can affect the mode and extent of absorption of RhB on the $PdCl_2/Bi_2WO_6$ surface and thus,

indirectly, the transformation rate of RhB. [30].

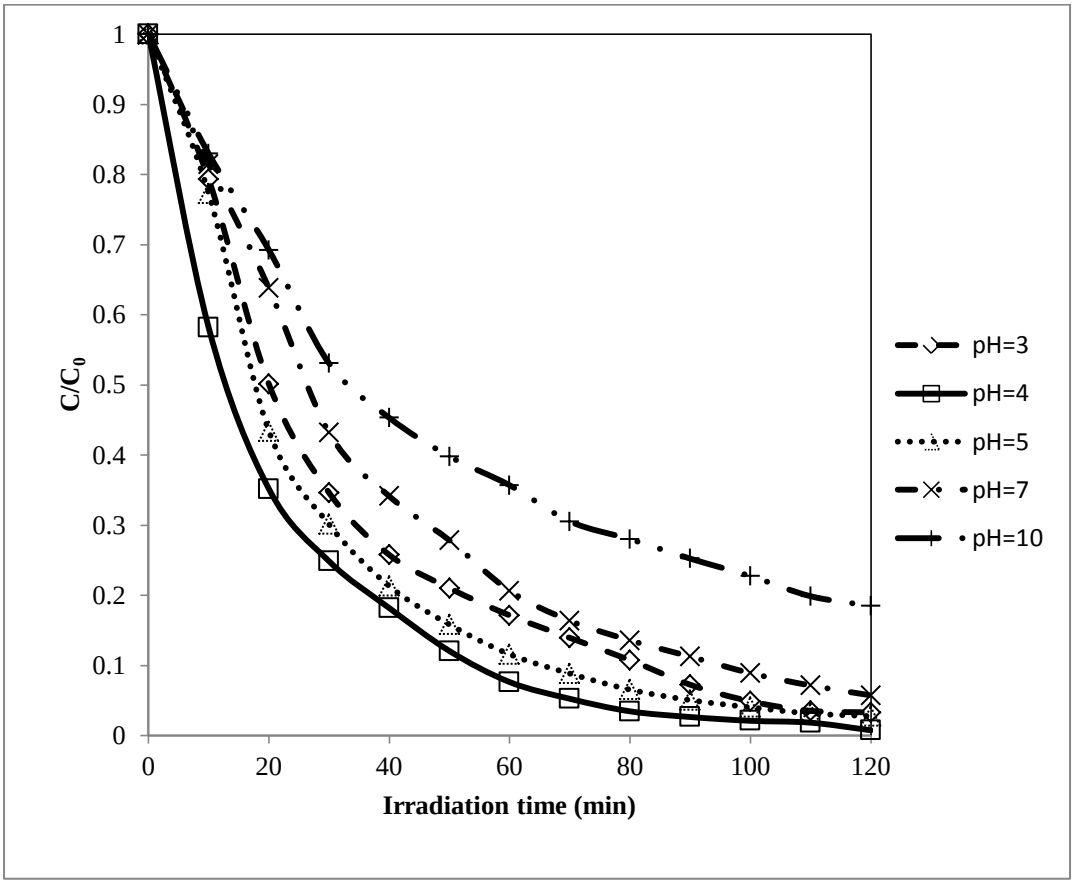

Figure 12 Effect of initial pH value of RhB solution on photocatalytic degradation

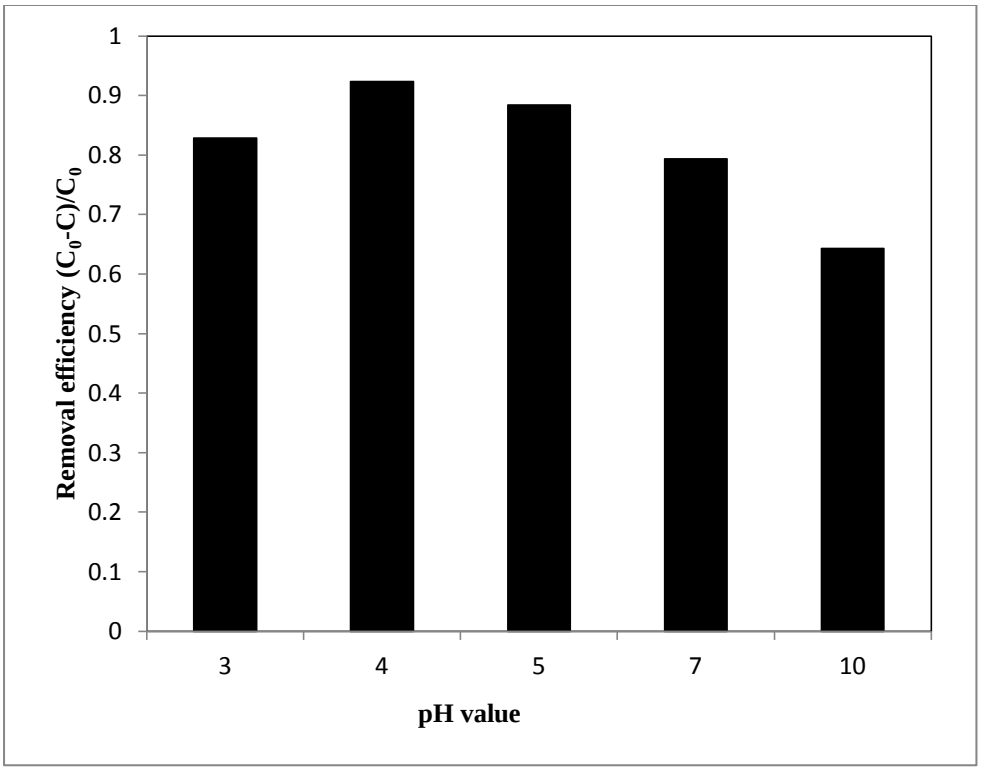

Figure 13 Effect of initial pH value of RhB solution on the removal efficiency within one hour degradation

3.3.7 Effect of initial RhB concentration

Figure 14 show the effect of the initial concentration of dye pollutant on removal efficiency. The influence of initial RhB solution concentration was studied from 5 mg/L to 150 mg/L when the dosage of $PdCl_2/Bi_2WO_6$ was 1 g/L. It can be observed from Figure 14 that the removal efficiency increased with an increase of initial RhB solution concentration from 5 mg/L to 10 mg/L and the removal efficiency decreased with the increasing of dye concentration from 10 mg/L to 150 mg/L. The decrease of removal efficiency from 10 mg/L to 150 mg/L can be attributable to the increasing of initial dye concentration causing competition for adsorption on the active sites on the photocatalyst, which decreased RhB degradation. Another reason was probably due to the light screening effect

of RhB solution [31].

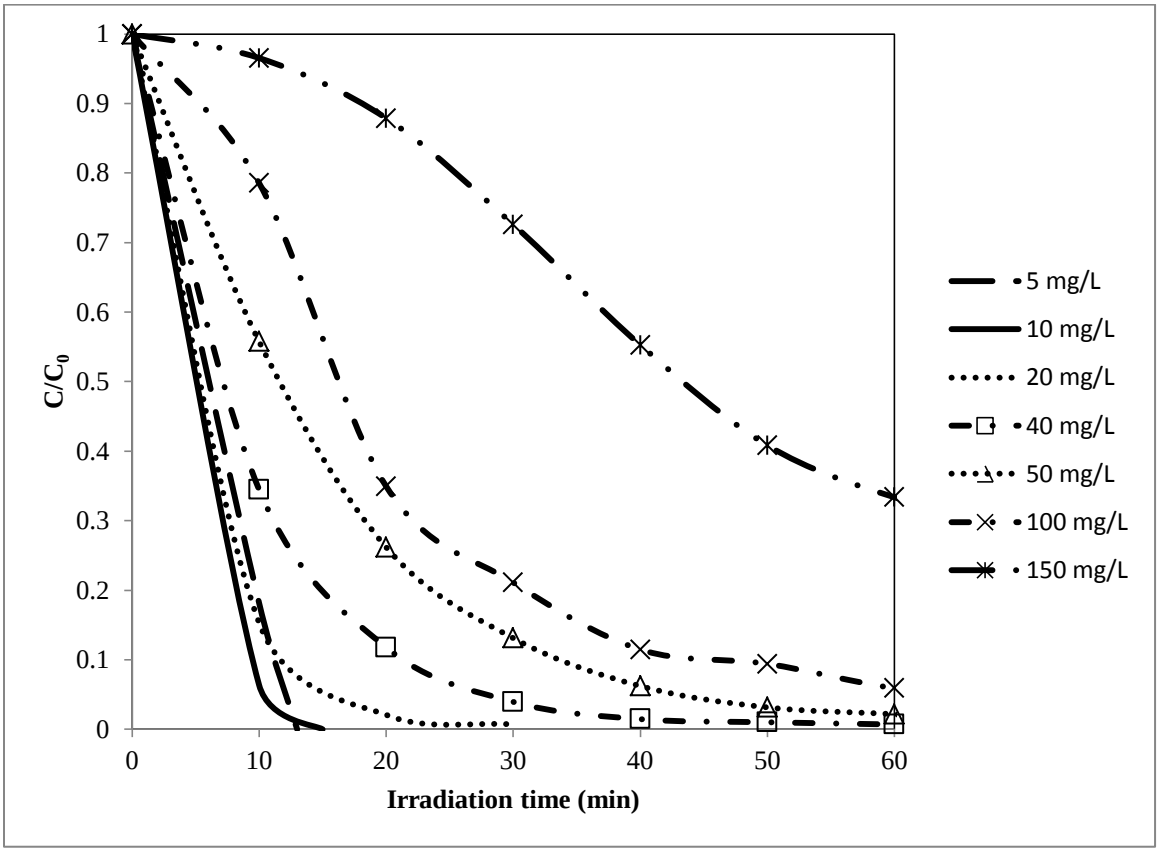

Figure 14 Effect of initial RhB concentration on the photocatalytic degradation within one hour degradation

3.3.8 Photocatalytic mechanism

In the photocatalytic reaction process, the excited electrons in the conduction band and positive holes in the valence band are produced when the $PdCl_2/Bi_2WO_6$ composite are irradiation under visible light. However, the photocatalytic efficiency depends on the surface charge transfer rate which is inhibited by the recombination of photogenerated electrons and the holes. To prevent this recombination, the loaded Pd acts as a charge receptor which traps the electron on the surface of Bi_2WO_6 and reduces to Pd(Ⅰ)Cl_2, and then transfers the electron to the O_2 molecules to return to the Pd(Ⅱ)Cl_2 state. Meanwhile,

since the standard redox potential of the valance band is more negative than the pairs of $\cdot OH/OH^-$, photogenerated hole does not react with OH^-/H_2O to form $\cdot OH$. So RhB molecules may directly react with the $O_2/O_2^{-\bullet}$ instead of react with free $\cdot OH$. The photocatalytic process as following [10]:

$$Bi_2WO_6 + hv \rightarrow Bi_2WO_6(e^- + h^+) \quad (1)$$

$$e^- + O_2 \rightarrow O_2^{-\bullet} \quad (2)$$

$$e^{-\bullet} + Pd(\text{Ⅱ})Cl_2 \rightarrow Pd(\text{Ⅰ})Cl_2 \quad (3)$$

$$Pd(\text{Ⅰ})Cl_2 + O_2 \rightarrow Pd(\text{Ⅱ})Cl_2 + O_2^{-\bullet} \quad (4)$$

$$RhB + O_2/O_2^{-\bullet} \rightarrow \text{products} \quad (5)$$

$$RhB + h^+ \rightarrow \text{products} \quad (6)$$

3.4. Conclusion

$PdCl_2/Bi_2WO_6$ hierarchical nanoparticles with different $PdCl_2$ loadings were prepared via a template free hydrothermal process, and photocatalytic activity was investigated by degradation of Rhodamine B. Compared to the pure Bi_2WO_6, $PdCl_2/Bi_2WO_6$ exhibited the higher photocatalytic activity, because of the synergetic effect between the transition metal and semiconductor. By XRD, XPS and SEM observations, it was found that the deposition of Pd species did not affect the morphology of Bi_2WO_6 photocatalyst. $PdCl_2$ doping on Bi_2WO_6 surface for the removal of RhB from solution exhibited an optimum value of 1 wt% Pd loading. The activity of $PdCl_2$ loaded Bi_2WO_6 was found to be a function of photocatalyst dosage, dye initial concentration and pH value of solution.

3.5. References

[1] J.M. Herrmann, Heterogeneous photocatalysis: Fundamentals and applications to the removal of various types of aqueous pollutants, Catalysis Today 53(1999) 115-129.

[2] A. Alinsafi, F. Evenou, E.M. Abdulkarim, M.N. Pons, O. Zahraa, A. Benhammou, A. Yaacoubi, A. Nejmeddine, Treatment of textile industry wastewater by supported photocatalysis, Dyes and Pigments 74(2007) 439-445.

[3] P. Pichat, J. Disdier, C. Hoang-Van, D. Mas, G. Goutailler, Gaysse, Purification/deodorization of indoor air and gaseous effluents by TiO_2 photocatalysis, Catalysis Today 63(2000) 363-369.

[4] H. Hidaka, Y. Suzuki, K. Nohara, S. Horikoshi, Y. Hisamatsu, E, Pellizzetti, Serpone, Photocatalyzed degradation of polymers in aqueous semiconductor suspensions. I. Photooxidation of solid particles of polyvinylchloride, Journal of Polymer Science, Part A: Polymer Chemistry 34(1996) 1311-1316.

[5] T. Matsunaga, R. Tomoda, T. Nakajima, Wake, Photoelectrochemical sterilization of microbial cells by semiconductor powders, FEMS Microbiology Letters 29 (1985) 211-214.

[6] Z. Cui, D. Zheng, T. Tang, J. Liu, C. Xie, Processing-structure-property relationships of Bi_2WO_6 nanostructures as visible-light-driven photocatalyst, Journal of Hazardous Materials 183(2010) 211-217

[7] A. Kudo, Hijii, H_2 or O_2 evolution from aqueous solutions on layered oxide photocatalysts consisting of Bi^{3+} with 6s2 configuration and d^0 transition metal ions, Chemistry Letters 10(1999) 1103-1104

[8] J. Tang, Z. Zhou, Ye, Photocatalytic decomposition of organic contaminants by

Bi_2WO_6 under visible light irradiation, Catalysis Letters 92(2004) 53-56

[9] X. Zhang, Y. Zhang, X. Quan, S. Chen, Preparation of Ag doped $BiVO_4$ film and its enhanced photoelectrocatalytic (PEC) ability of phenol degradation under visible light, Journal of Hazardous Materials 167 (2009) 911-914.

[10] F. Duan, Y. Zheng, M. Chen, Flowerlike $PtCl_4/Bi_2WO_6$ composite photocatalyst with enhanced visible-light-induced photocatalytic activity, Applied Surface Science 257 (2011) 1972-1978.

[11] M. Shang, W. Wang, L. Zhang, S. Sun, L. Wang, L. Zhou, Journal of Physical Chemistry C 113(2009) 14727-14731.

[12] J. Xu, W. Wang, E. Gao, J. Ren, L. Wang, Bi_2WO_6/Cu^0: A novel coupled system with enhanced photocatalytic activity by Fenton-like synergistic effect. Catalysis Communications 12 (2011) 834-838.

[13] D. Wang, G. Xue, Y. Zhen, F. Fu, D. Li, Monodispersed Ag nanoparticles loaded on the surface of spherical Bi_2WO_6 nanoarchitectures with enhanced photocatalystic activities. Journal of Materials Chemistry 22 (2012) 4751-4758.

[14] Q. Xiao, J. Zhang, C. Xiao, X.K. Tan, Photocatalystic degradation of methylene blue over Co_3O_4/Bi_2WO_6 composite under visible light irradiation, Catalysis Communications 9 (2008) 1237-1253.

[15] S.B Zhu, T.G. Xu, H.B. Fu, J.C. Zhao, Y.F. Zhu, Synergetic effect of Bi_2WO_6 photocatalyst with C-60 and enhanced photoactivity under visible irradiation. Environmental Science Technology 41 (2007) 6234-6239.

[16] L. Zhang, K. Wong, Z. Chen, J. Yu, J. Zhao, C. Hu, C. Chan, P. Wong, AgBr-Ag-Bi_2WO_6 nanojunction system: A novel and efficient photocatalyst with double

visible-light active components, Applied Catalysis A: General 363 (2009) 221-229.

[17] J. Ren, W. Wang, S. Sun, L. Zhang, J. Chang, Enhanced photocatalytic activity of Bi_2WO_6 loaded with Ag nanoparticles under visible light irradiation, Applied Catalysis B Environmental 92 (2009) 50-55.

[18] A. Magdziarz, M. A. Aramendia,A. Marinas, J. M. Marinas, F. J. Urbano, Navio, Influence of the strong metal support interaction effect (SMSI) of Pt/TiO_2 and Pd/TiO_2 systems in the photocatalytic biohydrogen production from glucose solution, Catalysis Communications 16 (2011) 1-6.

[19] S. Suh, J. Kim, S. Kim, B. Park, Effect of PI film surface on printing of Pd(Ⅱ)catalytic ink for electroless copper plating in the printed electronics, Journal of Industrial and Engineering Chemistry 18 (2010) 209-294.

[20] L. Ge, Synthesis and characterization of novel visible-light-driven $Pd/BiVO_4$ composite photocatalysts, Materials Letters 62 (2008) 926-928.

[21] A. Drelinkiewicz, J. Sobczak, E. Sobczak, M. Krawczyk, A. Zieba, A. Waksmundzka-Gora, Physicochemical and catalytic properties of Pt-poly(4-vinylpyridine) composites, Materials Chemistry and Physics 114 (2009) 763-773.

[22] Q. Xiao, J. Zhang, C. Xiao, X. Tan, Photocatalytic degradation of methylene blue over Co_3O_4/Bi_2WO_6 composite under visible light irradiation, Catalysis Communications 9 (2008) 1247-1253.

[23] L. Zhang, H. Wang, Z. Chen, P. Wong, J. Liu, Bi_2WO_6 micro/nano-structures: Synthesis, modifications and visible-light-driven photocatalytic applications, Applied Catalysis B: Environmental 106 (2011) 1-13.

[24] Y. Tian, G. Hua, W. Xu, N. Li, M. Fang,L. Zhang, Bismuth tungstate

nano/microstructures: Controllable morphologies, growth mechanism and photocatalytic properties, Journal of Alloys and Compounds 509 (2011) 724-730.

[25] L. Zhang, W. Wang, Z. Chen, L. Zhou, H. Xu, W. Zhu, Fabrication of flower-like Bi_2WO_6 superstructures as high performance visible-light driven photocatalysts, Journal of Materials Chemistry 17 (2007) 2526-2532.

[26] M. Gratel, Heterogeneous photochemical electron transfer, CRC Press, Baton Rouge, FL, 1998.

[27] X. Zhao, T. Xu, W. Yao, C. Zhang, Y. Zhu, Photoelectrocatalytic degradation of 4-chlorophenol at Bi2WO6 nanoflake film electrode under visible light irradiation, Applied Catalysis B: Environmental 72 (2007) 92-97.

[28] F. Amano, K. Nogami, B. Ohtani, Visible light-responsive bismuth tungstate photocatalysts: Effects of hierarchical architecture on photocatalytic activity, Journal of Physical Chemistry C (2009) 113, 1536-1542.

[29] M. Behnajady, B. Alizade, N. Modirshahla, Synthesis of Mg-Doped TiO_2 Nanoparticles under Different Conditions and its Photocatalytic Activity, Photochemistry and Photobiology (2011) 87, 1308-1314.

[30] J. Zhao, T. Wu, K. Wu, Photoassisted Degradation of Dye Pollutants. 3. Degradation of the Cationic Dye Rhodamine B in Aqueous Anionic Surfactant/TiO_2 Dispersions under Visible Light Irradiation: Evidence for the Need of Substrate Adsorption on TiO_2 Particles, Environmental science technology 32 (1998) 2394-2400.

[31] H. Guo, K. Lin, Z. Zheng, F. Xiao, S. Li, Sulfanilic acid-modified P25 TiO_2 nanoparticles with improved photocatalytic degradation on Congo red under visible light, Dyes and Pigments 92 (2012) 1278-1284.

Chapter 4. Effect of chemical reducing agents on Pd/Bi_2WO_6 and its visible light driven photocatalysis

Absorption

$Pd/Bi_2WO_6$was synthesized with improved visible light response and photocatalytic activity for degradation of Rhodamine B dye. The loaded Pd ions were subjected to chemical reduction using various reducing agents, including: CH_2O, N_2H_4 and $NaBH_4$.The size, structure, morphology and composition of the as-synthesized Pd/Bi_2WO_6 was determined by X-ray diffraction (XRD), X-ray photoelectron spectroscopy (XPS), scanning electron microscopy (SEM) and UV-Vis absorption spectra. It was found that the Pd did not alter the crystal structure of the Bi_2WO_6 host material. XPS analysis revealed that Pd in the CH_2O and N_2H_4-reduced composites was present in the form of both metallic and ionic Pd species (Pd^0 and Pd^{2+}). In the $NaBH_4$-reduced composite, the Pd was present only in the metallic state. The UV-vis spectrum of the Pd-loaded powders was red-shifted compared to pure Bi_2WO_6 and a band gap narrowing was observed. The photocatalytic activities of the samples were quantified by the degradation of RhB under visible light, and a maximum removal efficiency of 86.1% was obtained after 2 hours of irradiation.

4.1. Introduction

The eradication of environmental pollutants from wastewater effluents has become an emerging concern in recent decades. Every year a large amount of untreated or under-treated sewage is dumped into lakes, ponds, streams, rivers, estuaries and oceans. Sewage released from wastewater systems can contain concerning pollutants since even advanced treatment systems are unable to remove all pollutants and chemicals. Furthermore, many physical treatment techniques only transfer the pollutants from water to other phases. Therefore, a more effective technology is required. Photocatalysis offers a good treatment option, and can effectively degrade a wide range of pollutants, including organics such as dyes and also biological material such as bacteria and viruses [1]. Visible light composes 43% of the solar spectrum, which is ten times more than ultraviolet irradiation. In order to achieve the goal of effective solar utilization for photocatalysis, efforts have been focused on the development of highly efficient visible-light active photocatalysts.

Bi_2WO_6 is the member of the Aurivillius family with a layered structure comprising of the alternation of fluorite-like blocks and perovskite-like $(WO_4)_n^{2n-}$ [2]. The perovskite blocks include an infinite two-dimensional array of corner-linked WO_6 octahedra which alternate with $(Bi_2O_2)_n^{2+}$ slabs. The perovskite layers, which offer vacancies to a definite degree of oxide ions, lead to high oxide ion conductivity [3]. Figure 15 shows a schematic of the structures present in Bi_2WO_6.

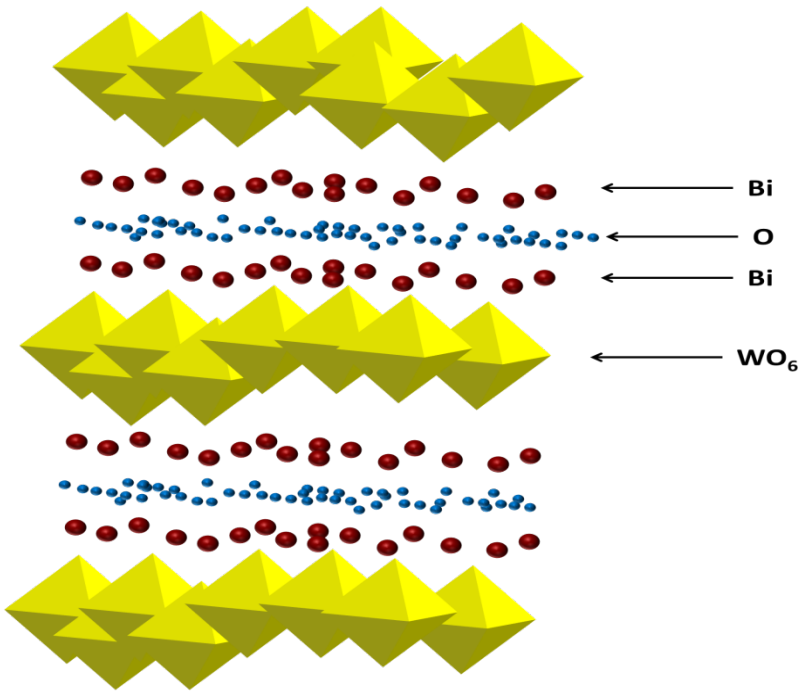

Figure 15 Structure of WO_4^{2-} and $Bi_2O_2^{2+}$ layers present in Bi_2WO_6 [4].

Several studies found that the visible light absorption of Bi_2WO_6 is attributed to the transition from Bi 6s to the W 5d orbital, where Bi 6s and O 2p bands are hybridized to form the valence band of each oxide [1]. Due to its unique physical and chemical properties, Bi_2WO_6 has been found to have excellent photocatalytic activity under visible light [5, 6, 7, 8].

Despite this, the low efficiency for hydrogen production of Bi_2WO_6 restricts its large-scale application due to [9] the quick rate of recombination for electron-hole pairs observed in the bulk or on the face of Bi_2WO_6 particles, and the quick reverse reaction of oxygen and hydrogen to form water on the surface of Bi_2WO_6 [10]. To overcome these limitations, some studies modified Bi_2WO_6 with other semiconductors or metal such as TiO_2 [11], Co_3O_4 [12], Fe_3O_4 [13], and AgBr-Ag-Bi_2WO_6 nanojunction-type structures [14]. However, most of studies modified Bi_2WO_6 with salts, such as sulphate, chloride,

and phosphate. These inorganic anions were found to be rapidly adsorbed by the photocatalysts and decreased the observed oxidation rate by 20% to 70%, which limited the photocatalytic performance of the composites. It has been found that the presence of inorganic anions on the photocatalyst may compete with the organic pollutants for surface active sites and form a highly polar environment near the particle surface, which would block the diffusion of organics to the active sites. To eliminate this shortcoming, we doped small quantities of metallic metal on the photocatalyst instead of salt. It has been reported that the metallic metal can improve the efficiency of photoredox transformations, and simultaneously reduce the negative impact of the salts [15, 16, 17]. Considering this, we designed a composite photocatalyst consisting of metal nanoparticles loaded on Bi_2WO_6. Some studies have reported the conversion of metal ions to metal nanoparticles by using thermal, photochemical, radiolytic, and chemical reductions [18]. Compared to the first three methods, the chemical method is widely applicable to many systems. Ryu et al. synthesized Pt-Ru doped PThB catalyst using $NaBH_4$ as reducing agent, and this material showed enhanced electrocatalytic oxidation of CO and methanol [19]. Hajek et al. studied the influence of chemical reduction on the properties of bimetallic Ru-Sn/SiO_2 catalyst. These sol-gel catalysts were reduced by $NaBH_4$, KBH_4, H_2 and CH_2O. It was found that, of the prepared materials, the $NaBH_4$-reduced catalyst exhibited the highest activity and selectivity [20]. In this study, we prepared Pd/Bi_2WO_6 composite photocatalysts, and investigated the effect of various chemical reduction processes using $NaBH_4$, CH_2O and N_2H_4 as reducing agents, respectively. The photocatalytic activities of the composite photocatalysts prepared were investigated for the degradation of Rhodamine B under visible light irradiation. It was found that the Pd/Bi_2WO_6 exhibited a higher photo-

catalytic activity than the pure Bi_2WO_6 alone. Among the composites prepared, it was found that the $NaBH_4$-reduced catalyst exhibited the highest activity and the best optical absorption in the visible light region.

4.2. Experimental

4.2.1 Synthesis of Bi_2WO_6 photocatalyst by hydrothermal method

Bi_2WO_6 samples were prepared using a hydrothermal method. Typically, 0.98 g of $Bi(NO)_3 \cdot 5H_2O$ (ACS reagent grade, 98%, supplier) was dissolved in 40 mL acetic acid, 0.33 g of $Na_2WO_4 \cdot 2H_2O$ (purum grade, 99%, supplier) was dissolved in 20 mL deionized water, and added dropwise to the above $Bi(NO)_3$ solution under magnetic stirring for 30 minutes. The pH value of the suspension was adjusted to 1 using hydrochloric acid solution (0.5 mol/L, Sigma Aldrich), and the mixture was sealed in a Teflon-lined stainless steel autoclave at 60% of its maximum volume and heated 180^{o}C for 20 hours, and then cooled to room temperature. The resulting sample was filtered and washed twice with deionized water. Finally, the samples were dried in an oven at 80^{o}C for 2 hours.

4.2.2 Preparation Pd/Bi_2WO_6 composite photocatalysts

Scheme 1 shows the procedure used to prepare the Pd/Bi_2WO_6 composite photocatalysts. For the metal loading process, the $PdCl_2$-loaded Bi_2WO_6 composite sample was first prepared by an isometric impregnation method. A calculated concentration of $PdCl_2$ solution was added to 0.5 g Bi_2WO_6 to obtain a final mass percent of 1.0 wt%. It should be noted that, in our previous study, we found the optimum value of Pd loading amount to be 1 wt%. The suspension was then stirred using a glass rod and dried in ambient air. The resulting powder was collected and heated in the oven at 80^{o}C for 2 hours. For the reduc-

tion process, 0.25 mL N_2H_4, $NaBH_4$ or CH_2O solution was employed as a reducing agent and was added dropwise into 0.5 g Pd/Bi_2WO_6, respectively. The chemical reducing agents were allowed to reduce the metal ions at room temperature for 10 minutes under stirring. The suspension was then filtered and washed twice with deionized water thoroughly. Finally, the samples were dried at room temperature. Figure 16 shows a flow chart for the synthesis of Pd/Bi_2WO_6 composite photocatalysts.

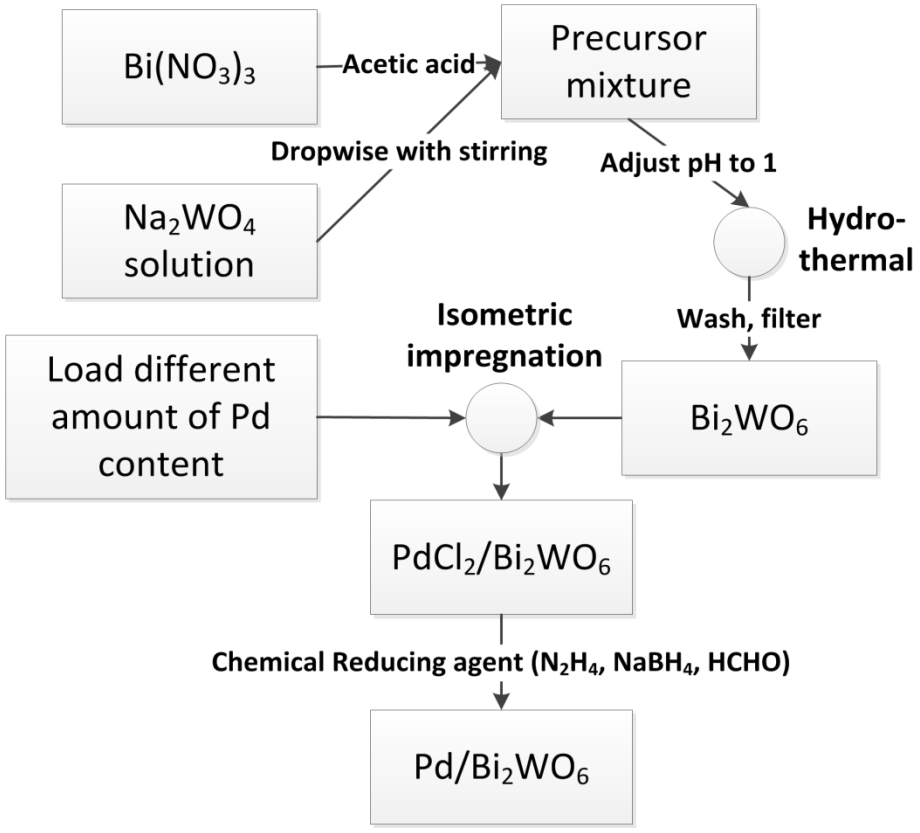

Figure 16 Flow chart for synthesis of Pd/Bi_2WO_6 composite photocatalysts

4.2.3 Characterization

Particle size and morphology was investigated using the scanning electron microscope images (SEM) (JEOL JSM-7500F). The structure characterization of the samples was carried out by studying the X-ray diffraction (XRD) patterns (Rigaku Ultima IV). For the

XRD analysis, the wavelength of X-ray radiation used was 0.15418 nm, and the XRD spectra of the samples were collected over the range of $2\theta = 10^{o}$ to 80^{o}. The chemical states of the elements in samples were investigated by X-ray photoelectron spectra (XPS) (Kratos Axis Ultra). The optical absorption properties of samples were recorded on the ultraviolet visible light diffuse reflectance spectra (UV-vis DRS) (Puxi, UV1901).

4.2.4 Photocatalytic activity

To quantify the photocatalytic degradation of Rhodamine B (RhB) under visible light, given amounts of Pd/Bi_2WO_6 powders were dispersed in a Pyrex reactor containing 100 mL of aqueous solution of RhB (Sigma-Aldrich). Illumination was provided by a 300 W tungsten halide bulb (Ushio) which was filtered through a 420 nm UV cut-off filter (Kenko Zeta, transmittance>90%) at a distance of 10 cm from the reactor. The irradiation was quantified using a quantum meter (Biospherical QSL-2100; 400 nm$<\lambda<$700 nm). The incident photon flux was approximately $4.7*10^{-3}$ Einstein/m^2/s. The sensor had a nominal sensitivity of 1 volt with a noise level less than 1 mV. The cooling/heating recirculating water was provided using an external cooling jacket to control the temperature of the reaction around $20^{o}C\pm2$. The pH value of the mixture was adjusted by either sodium hydroxide (0.5 mol/L, Sigma-Aldrich) or hydrochloric acid solution (0.5 mol/L, Sigma-Aldrich). A 100 mg/L RhB solution was allowed to equilibrate in the dark with 1 g/L of catalyst under constant magnetic stirring at 280 rpm for 30 minutes prior to each experiment to achieve adsorption/desorption equilibrium. Each photocatalytic degradation test was performed for 2 hours with 1mL of sample drawn at given time intervals (every 10 minutes). The samples were centrifuged (12000 rpm, 3 minutes) to separate the photocatalysts in a Micro 17 (Fisher Scientific) microcentrifuge. The reaction solution ab-

sorbance was measured by a Genysys 10-UV spectrophotometer (Geneq Inc.) with the peak adsorption at $\lambda = 552$ nm. The absorbance was correlated to RhB concentration using the Beer-Lambert Law and a prepared calibration curve. Control runs were performed in the absence of light and photocatalysts, respectively. All runs were performed in triplicate.

4.3. Results and discussion

4.3.1 SEM observation

Light absorption and photochemical reactions both take place on the surface of photocatalysts, so the surface structure plays an important role in photocatalysis with respect to generation, transport, and reduction/oxidation of reactive species. To study these structures, SEM was used to study the morphology of the sample surfaces. Figure 17 represents SEM images of Pd/Bi_2WO_6 composite photocatalysts reduced by CH_2O, N_2H_4 and $NaBH_4$. As shown in Figure 17, all samples have an approximately spherical morphology, with diameters ranging from 7 to 10 μm. Further magnification of an individual sphere showed that the sample was constructed from a large quantity of two-dimensional nanosheets with sizes of approximately 100-200 nm, which were closely packed and formed a hierarchical structure. The SEM images of Pd/Bi_2WO_6 composite photocatalyst reduced by a chemical reducing agent (shown in Figure 17a, c and e) had a similar constructure and morphology. However samples prepared using N_2H_4 and CH_2O reductants showed a larger size distribution and were more agglomerated than those prepared using $NaBH_4$ during the reduction process. It is reported that small grain size and large specific surface area photocatalysts demonstrate higher photocatalytic activity, since they can fa-

cilitate electron hole separation and increase the number of active sites [21].

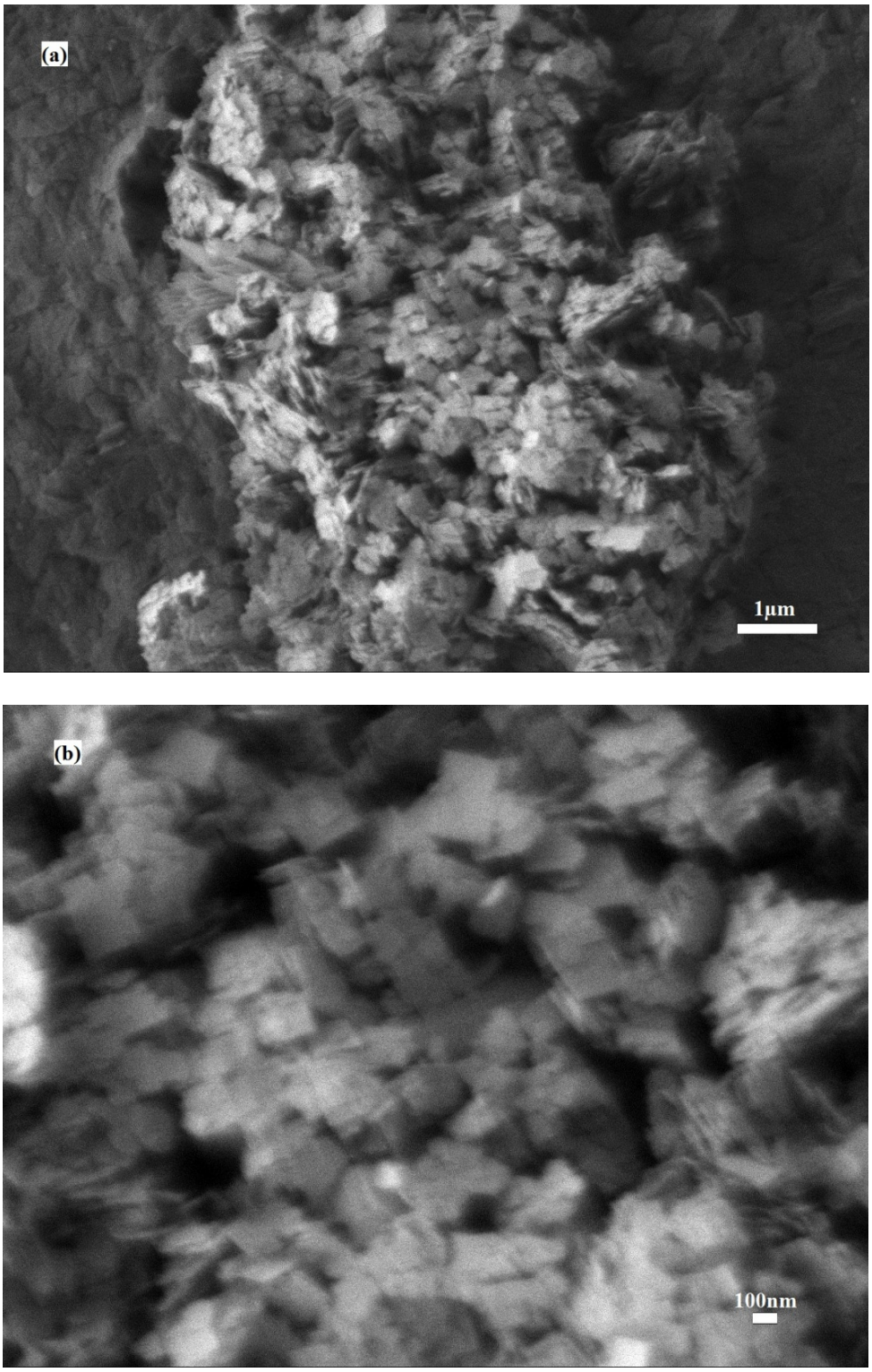

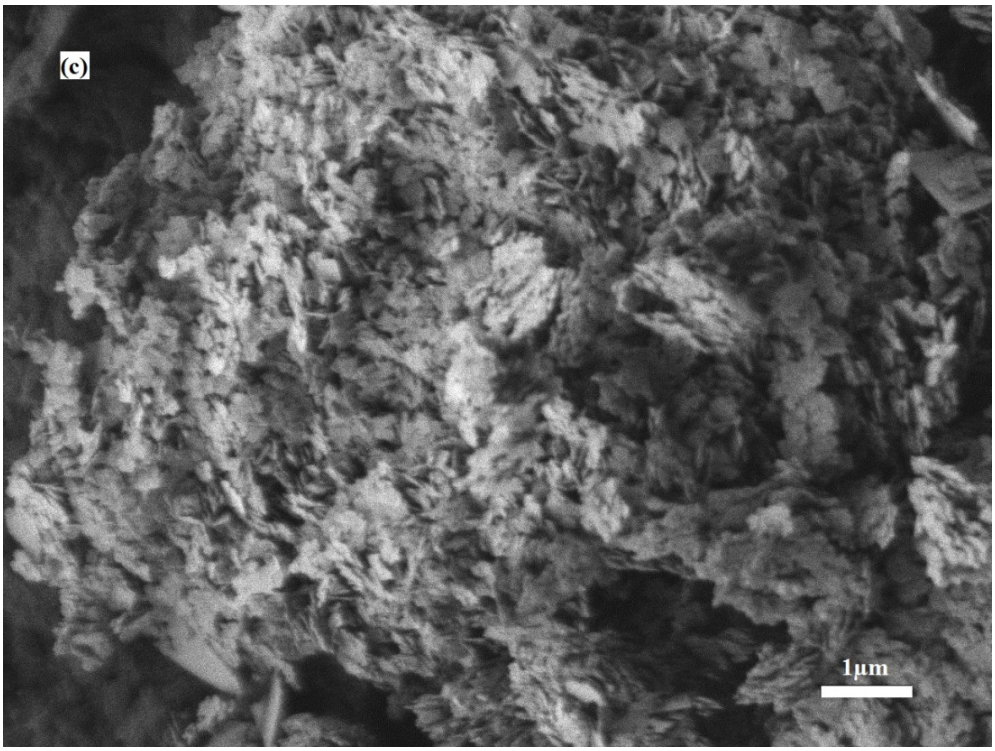
(c)
1μm

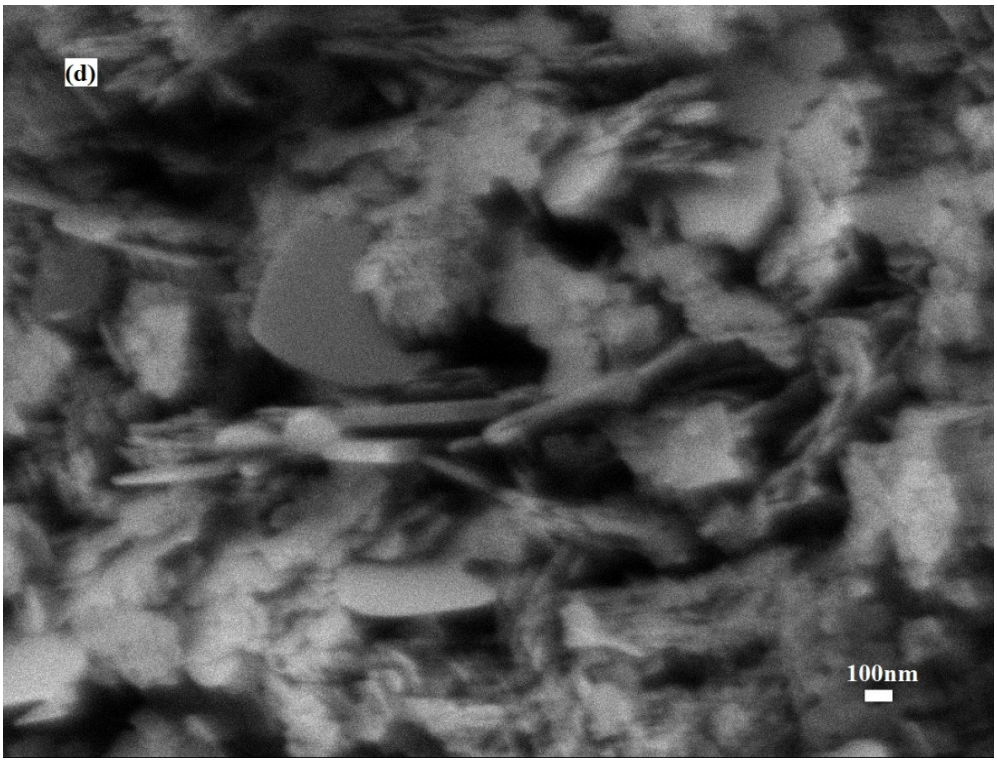
(d)
100nm

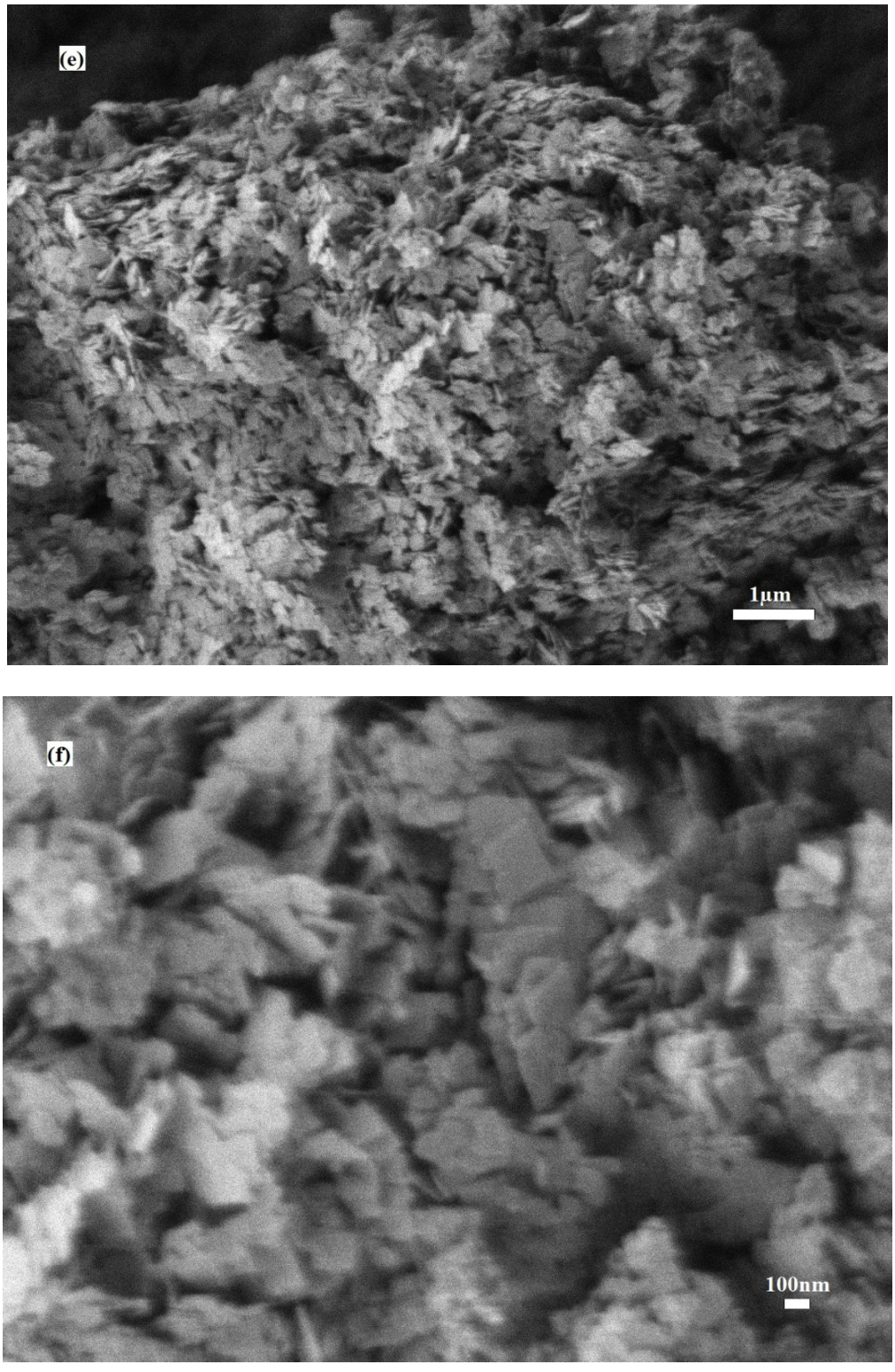

Figure 17 SEM images of the Pd/Bi_2WO_6 samples reduced by $NaBH_4$ (a) and (b), N_2H_4 (c) and (d), and CH_2O (e) and (f).

4.3.2 XRD analysis

The crystal structure of the photocatalysts was investigated using XRD measurements. As shown in Figure 18, Bi_2WO_6 was present as the orthorhombic phase corresponding to DB Card No.: 01-075-5628. No other peaks related to possible impurities were detected. From the XRD data, it was seen that Pd-modified Bi_2WO_6, prepared through the isometric impregnation and chemical reduction process did not affect the crystal structure of the host Bi_2WO_6 photocatalyst. Moreover, the absence of a peak corresponding to Pd could be attributable to the small content of Pd species introduced as well as high dispersion of metal ion deposits on the surfaces of Bi_2WO_6 [22].

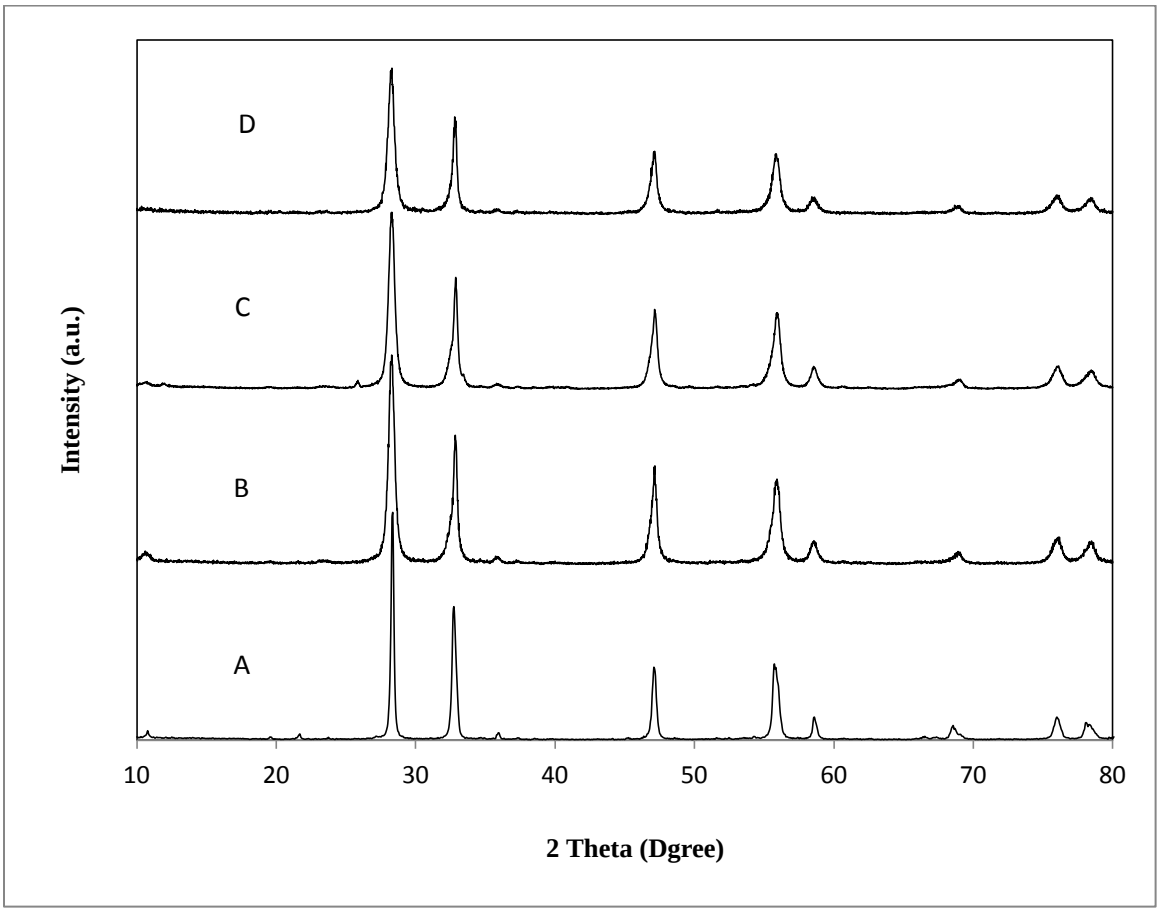

Figure 18 XRD patterns of pure Bi_2WO_6 (A) and different samples reduced by CH_2O (B), N_2H_4 (C) and $NaBH_4$ reductants (D)

4.3.3 XPS analysis

XPS analysis was carried out in order to determine the chemical elemental composition and valence states of the surface elements. Figure 19-Figure 22 showed the XPS spectra obtained by scanning Pd 3s (Figure 19), Bi 4f (Figure 20), W 4f (Figure 21) and O 1s levels (Figure 22) for the various samples prepared, respectively. The presence and valence state of the Pd species was mainly observed by XPS. For the CH_2O-reduced composite, four peaks corresponding to binding energies of 333.9 eV, 336 eV, 339 eV and 341.5 eV were observed, and were assigned to the Pd $3d_{5/2}$ and Pd $3d_{3/2}$ orbital according to the literature [23]. It is known that metallic Pd^0 has binding energies around 334.9 eV while palladium in positive ions such as Pd^{2+} exhibits higher binding energy around 336.4 eV (for Pd $3d_{5/2}$). So the two peaks around 336 eV and 341.6 eV indicated the presence Pd^{2+} species [24]. Weak satellite peaks beside the Pd^{2+} peaks were detected, and indicated the existence of Pd^0 in a very low concentration. In this case, a new Pd reagent containing zero valent Pd and Pd ions was present on the Bi_2WO_6 surface, and the concentration of Pd^{2+} ions was greater than the metallic Pd^0 species. For the N_2H_4-reduced composite, the Pd 3d orbit exhibited four peaks at 333.3 eV, 335.6 eV, 338.8 eV and 341.1 eV, respectively. The peaks as 333.4 eV and 338.8 eV were attributed to the spin orbit of Pd^0. The weak satellite peaks at 335.6 eV and 341.1 eV were attributed to the Pd^{2+} species, and were less intense than the Pd^0 species. For the $NaBH_4$-reduced composite, the binding energies for Pd $3d_{5/2}$ and Pd $3d_{3/2}$ were observed at 338.6 eV and 333.4 eV, indicating that palladium species was present as zero valent Pd. Compared to N_2H_4 and CH_2O, $NaBH_4$ is known to be most active reducting agent, which is intensely reactive in aqueous environment at room temperature. Moreover, CH_2O can only moderately react in aqueous solution and is a weaker reducing agent than N_2H_4. However, a complete

reduction of Pd species by both N_2H_4 and CH_2O can be barely be attained. The XPS spectrums of Bi 4f for various samples were shown in Figure 20. All of the samples showed a similar doublet around 163 eV and 158 eV, which was attributed to the spin orbit components of Bi $4f_{7/2}$ and Bi $4f_{5/2}$. A spin orbit splitting energy between Bi $4f_{7/2}$ and Bi $4f_{5/2}$ was found to be approximately 5.5 eV, which revealed a trivalent oxidation state of bismuth [22, 25]. As shown in Figure 21, the binding energies for W $4f_{7/2}$ and W$4f_{5/2}$ of all samples were observed around 36 eV and 34 eV, indicating a W^{6+} oxidation state for tungsten. The XPS peaks for the O 1s level of all the samples are shown in Figure 22. The peaks centered at the binding energy of 529 eV demonstrated that the oxygen species was present as lattice oxygen [26].

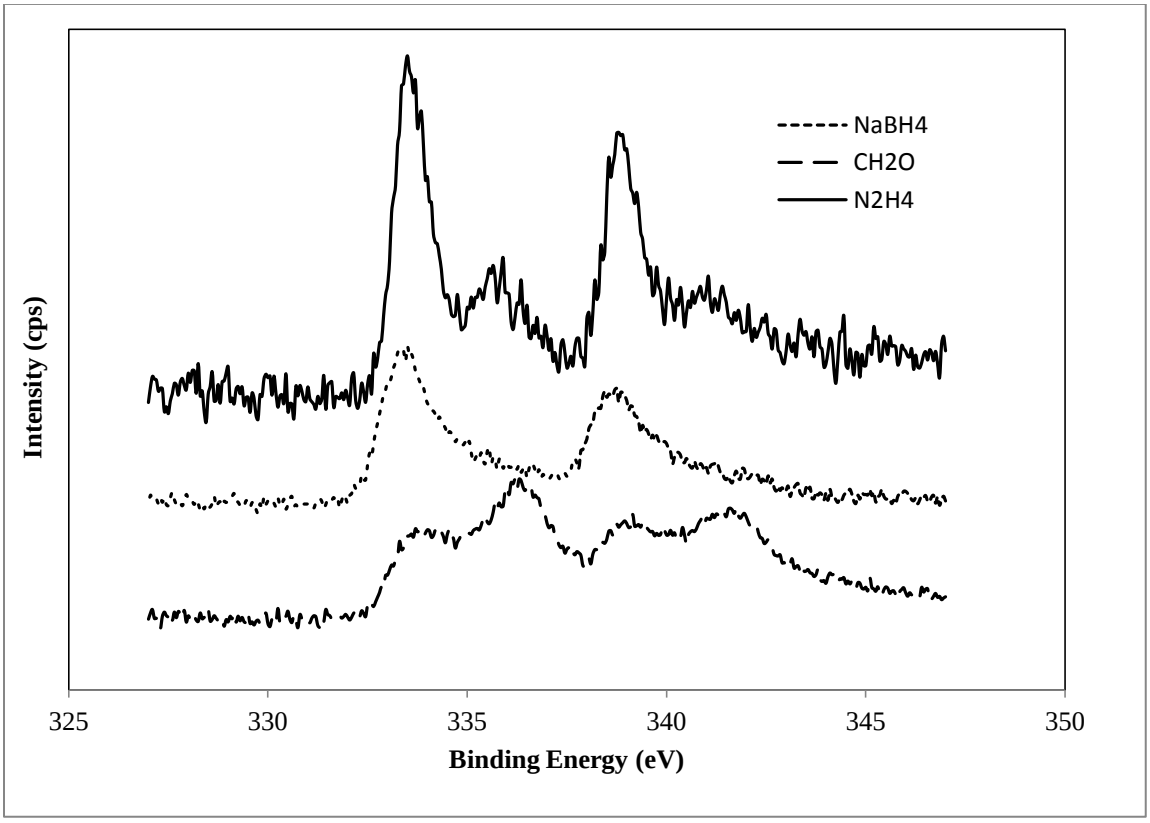

Figure 19 XPS spectra of Pd 3d orbit in Pd/Bi_2WO_6 composites prepared by CH_2O, N_2H_4, $NaBH_4$ reductants

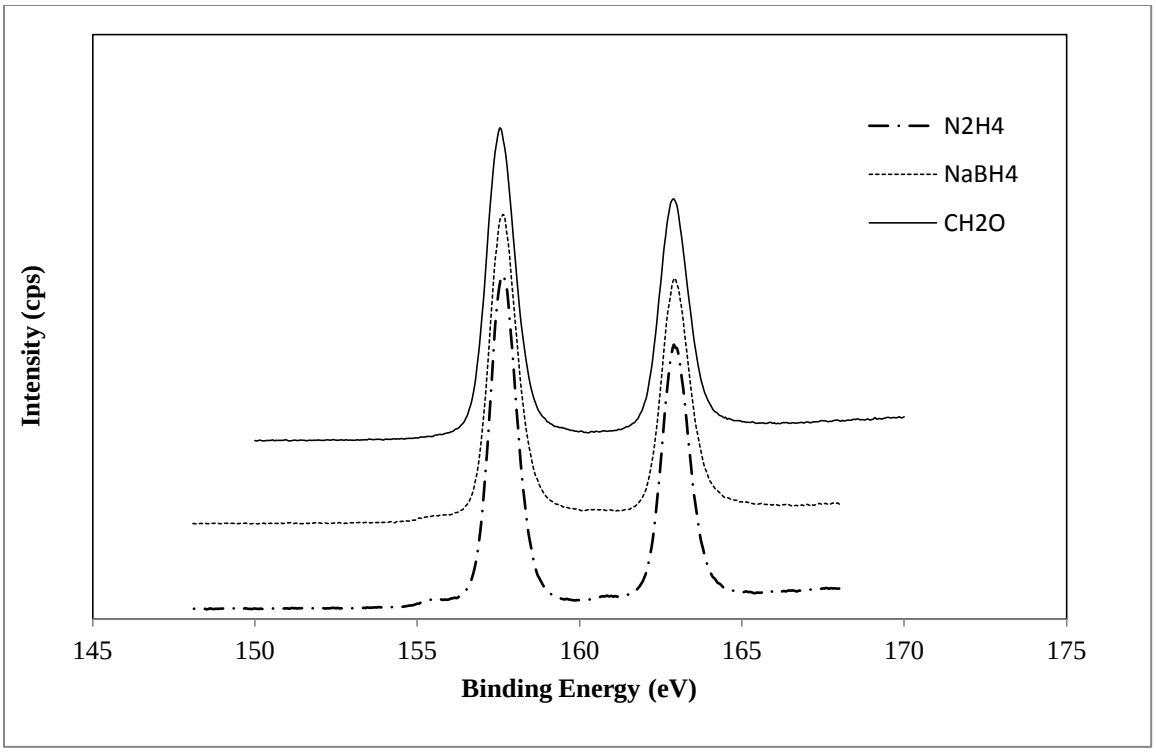

Figure 20 XPS spectra of Bi 4f orbit in Pd/Bi_2WO_6 composites prepared by CH_2O, N_2H_4, $NaBH_4$ reductants

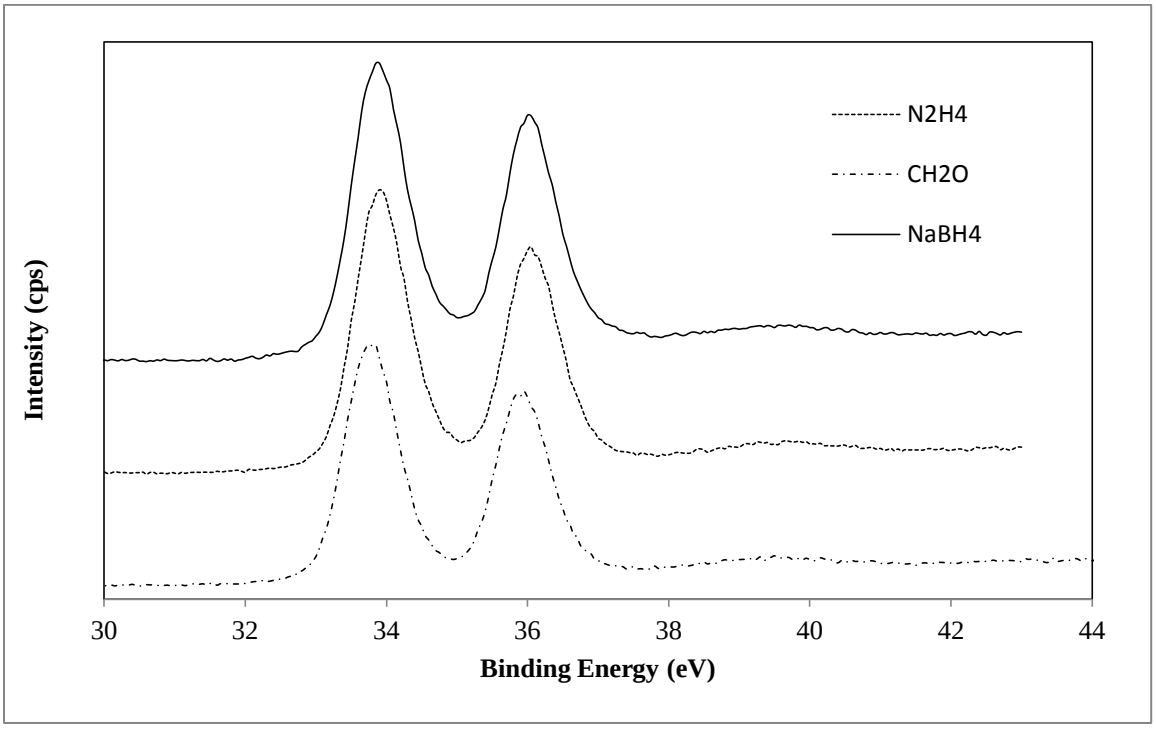

Figure 21 XPS spectra of W 4f orbit in Pd/Bi_2WO_6 composites prepared by CH_2O, N_2H_4,

$NaBH_4$ reductants

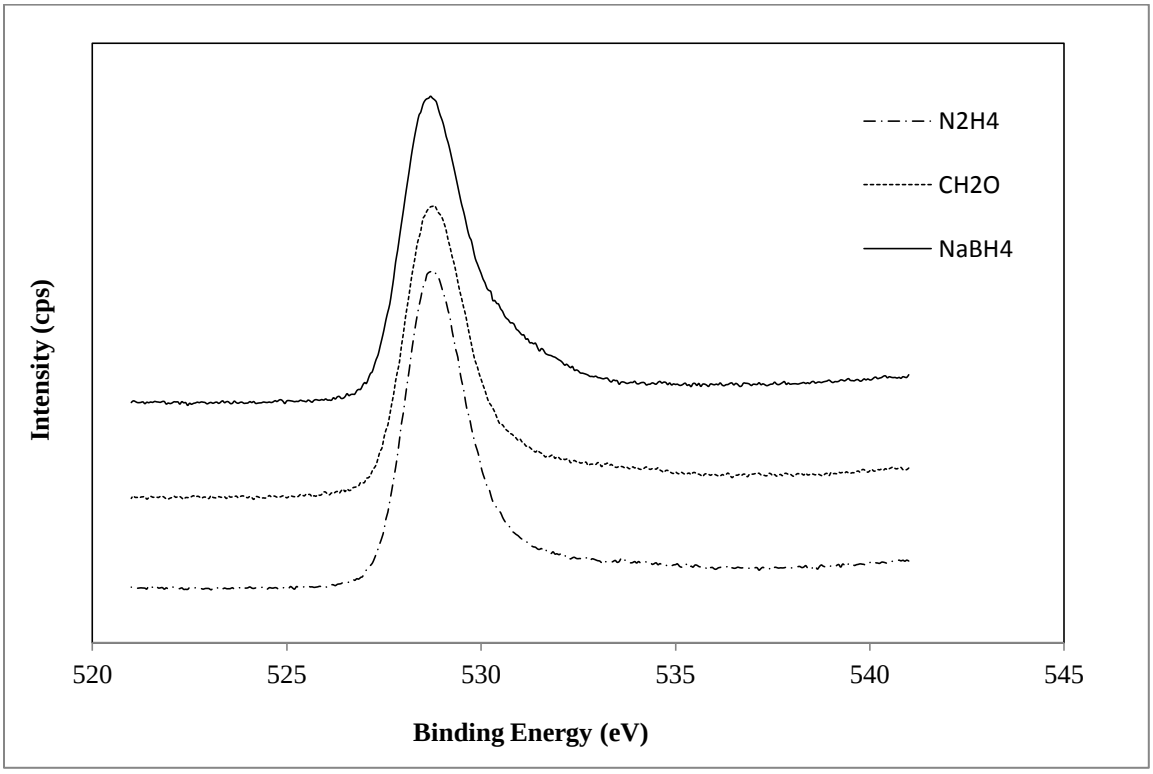

Figure 22 XPS spectra of O 1s orbit in Pd/Bi_2WO_6 composites prepared by CH_2O, N_2H_4, $NaBH_4$ reductants

Table 5 Contents of Pd, Cl species in Pd/Bi_2WO_6 composite photocatalyst

Sample	**Pd Atomic Concen-tration (%)**	**Cl Atomic Concentration (%)**
CH_2O – reduced composite	1.83	3.54
N_2H_4 – reduced composite	1.81	3.05
$NaBH_4$-reduced composite	0.95	0.88

The surface elemental composition was probed using XPS. The approximate compositions are given in Table 5. From the table, it can be seen that the $NaBH_4$ was the strongest reducing agent, compared to the other reductants, due to the atomic ratios of the Pd and Cl observed. This corresponded well with the valence states observed from the XPS data. However, a complete reduction of Pd species by $NaBH_4$ was not attained. The indicated decrease in Pd loading was also indicative of possible leaching of Pd ions during the washing procedure.

4.3.4 UV-vis diffuse absorption spectra

The UV-vis diffuse reflectance spectra were performed to compare the absorbance spectrum of different Pd/Bi_2WO_6 samples. The band gap energy was calculated by the following formula:

$$\lambda = 1240/E_g \quad (1)$$

where λ is the wavelength (nm) and Eg is the band gap energy (eV) [23]. The pure Bi_2WO_6 exhibits photo-absorption properties from the UV light region approximately 460 nm (in the visible light region) due to the intrinsic band-gap transition, corresponding to a band gap of 2.69 eV [102]. The band gap of samples prepared by N_2H_4, formaldehyde and $NaBH_4$ were 2.64 eV, 2.61 eV and 2.38 eV, respectively. Compared to pure Bi_2WO_6, all three composite samples prepared showed a decrease in the band gap energy and an improvement in visible light absorption. The visible light absorption of the composite photocatalysts was significantly improved by Pd loading and the absorption edge shifted to the visible light range.

According to the diffuse reflection spectrum shown in the Figure 23, the Pd/Bi_2WO_6 photocatalysts prepared using CH_2O and N_2H_4 exhibited photo-absorption from the UV

to the visible light regions, exhibiting absorption up to approximately 470 nm and 475 nm, respectively. Compared to pure Bi_2WO_6, the photo-absorption was red-shifted due to loading with Pd species, which caused the formation of metallic Pd and Pd^{2+} ion phases in the prepared Bi_2WO_6 host and introduced closely situated acceptor levels in the forbidden gap of the Bi_2WO_6. Domaradzki et al. doped TiO_2 thin film by Pd species, and found that the additional energy level created by the doping species was lower than the band gap, which caused the formation of metallic Pd and PdO phase [24]. The onset of absorption spectrum of the sample prepared by $NaBH_4$ was found to be around 520 nm. From the XPS analysis, it was previously found to be mainly metallic Pd loaded Bi_2WO_6. The adsorption band from 460 nm to 520 nm in the visible light region could be possibly attributed to the surface plasmon band of the metallic Pd. Surface plasmon absorption in metal nanoparticles occurs from the collective oscillations of the free conduction band electrons that are enhanced by incident electromagnetic radiation. Wang et al. modified Bi_2WO_6 by depositing Ag on the surface, and the visible light region absorption could be attributed to the surface plasmon band of the Ag nanoparticles [27]. Xiao et al. found that nano-palladium has a surface plasmon response band in the visible light, and suggested various optical applications such as novel supported photocatalysis [28]. Kanchana et al. found that the broad surface plasmon peak for the metallic Pd nanoparticles in size ranging from 2 to 100 nm was approximately at 320 nm, and with the increase in the particle size, the optical absorption spectra of metal nanoparticles that are dominated by surface plasmon resonances may shift towards longer wavelengths. Therefore the position of absorption band also strongly depends upon dielectric constant of the medium and surface-adsorbed species [29].

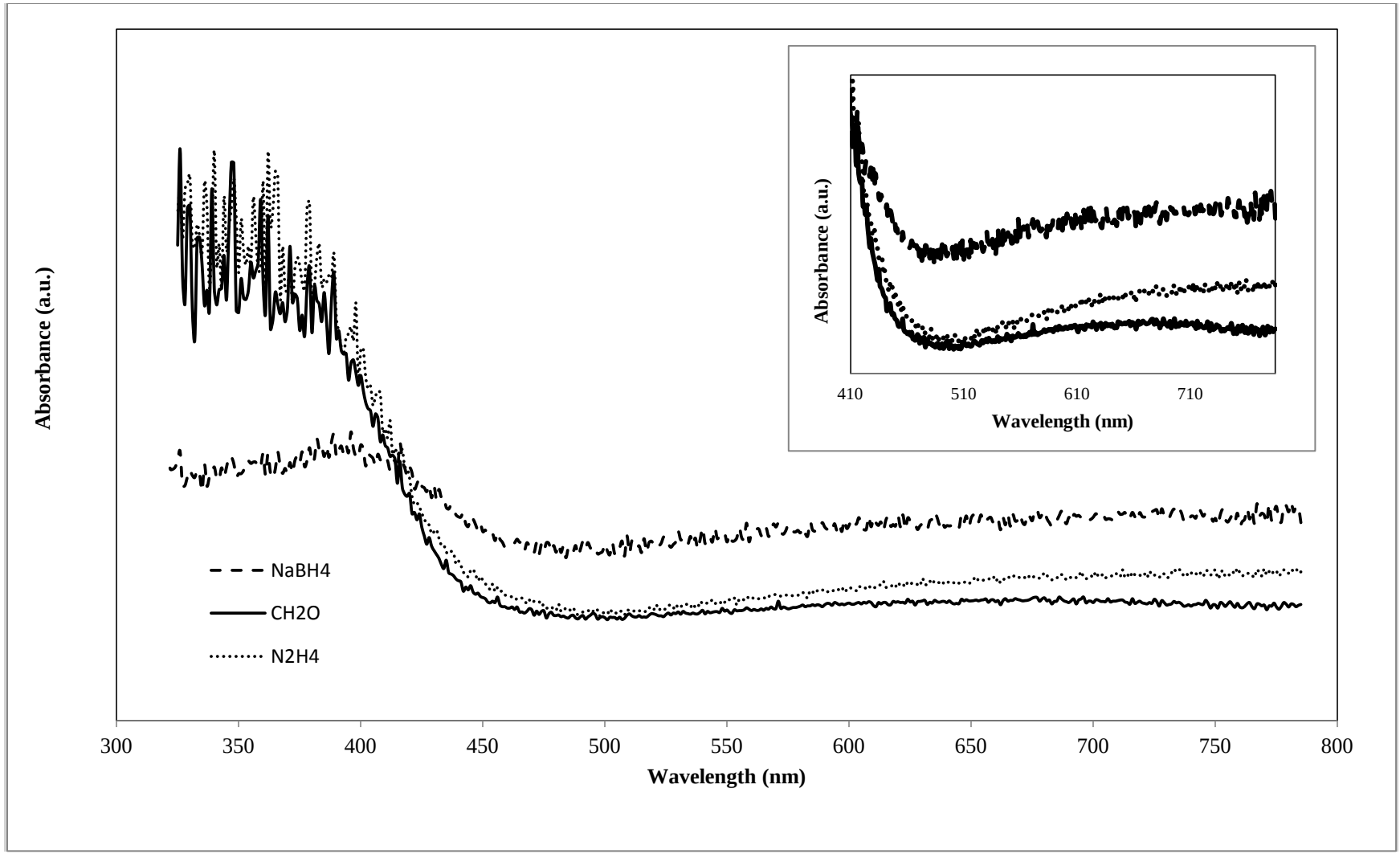

Figure 23 UV-vis diffuse absorption spectra of Pd/Bi_2WO_6 composite prepared by $NaBH_4$, CH_2O and N_2H_4 reductants.

4.3.5 Photocatalytic degradation of RhB

The photocatalytic activity was evaluated through the degradation of Rhodamine B (RhB) in aqueous solution under visible light irradiation. For comparison, the photocatalytic performance of pure Bi_2WO_6 was investigated under the same conditions as that of the Pd/Bi_2WO_6 composite samples prepared using various chemical reductants. The contaminant RhB was stable when adsorption-desorption equilibrium was achieved in absence of illumination for 30 minutes. It was found that the Pd loaded Bi_2WO_6 could efficiently improve the photocatalytic activity for the degradation of RhB solution when the Pd content was relatively low. Figure 24 and Figure 25 showed the photocatalytic performance of various Pd/ Bi_2WO_6 prepared. The results were quantified in terms of the removal of RhB from solution. The photocatalytic degradation efficiency was calculated using the equation [30],

$$\text{Degradation efficiency}(\%) = \frac{C_0 - C}{C_0} * 100\% \quad (1)$$

where C_0 is the initial concentration of Rhodamine B (mg/L) and C is the concentration (mg/L) at any time t (min) during the degradation.

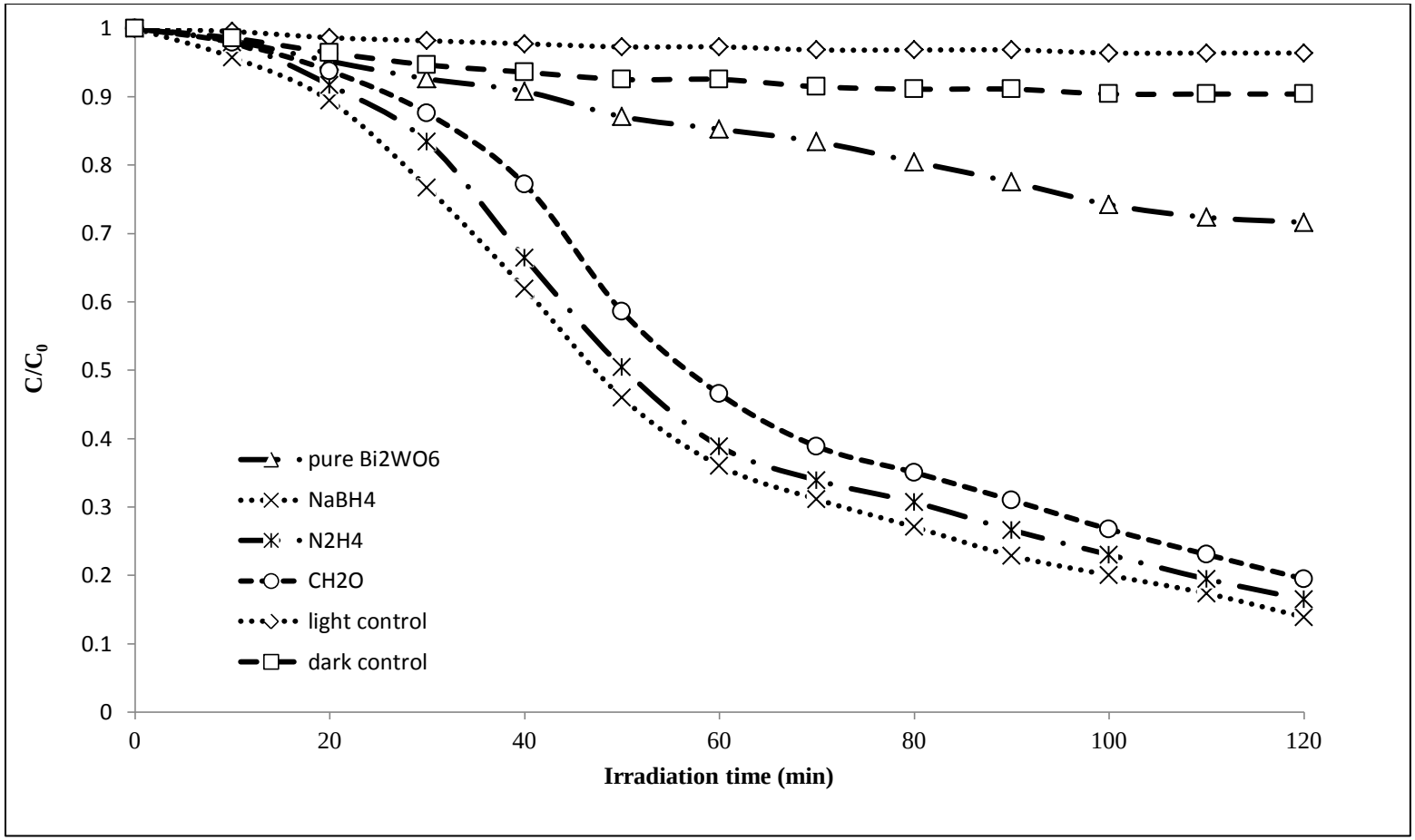

Figure 24 Normalized RhB concentration during the course of reaction using various photocatalysts: (a) pure Bi_2WO_6 (b) $NaBH_4$ reduced composite (c) N_2H_4 reduced composite (d) CH_2O reduced composite (e) light control (without photocatalyst) (f) dark absorption (without lamp)

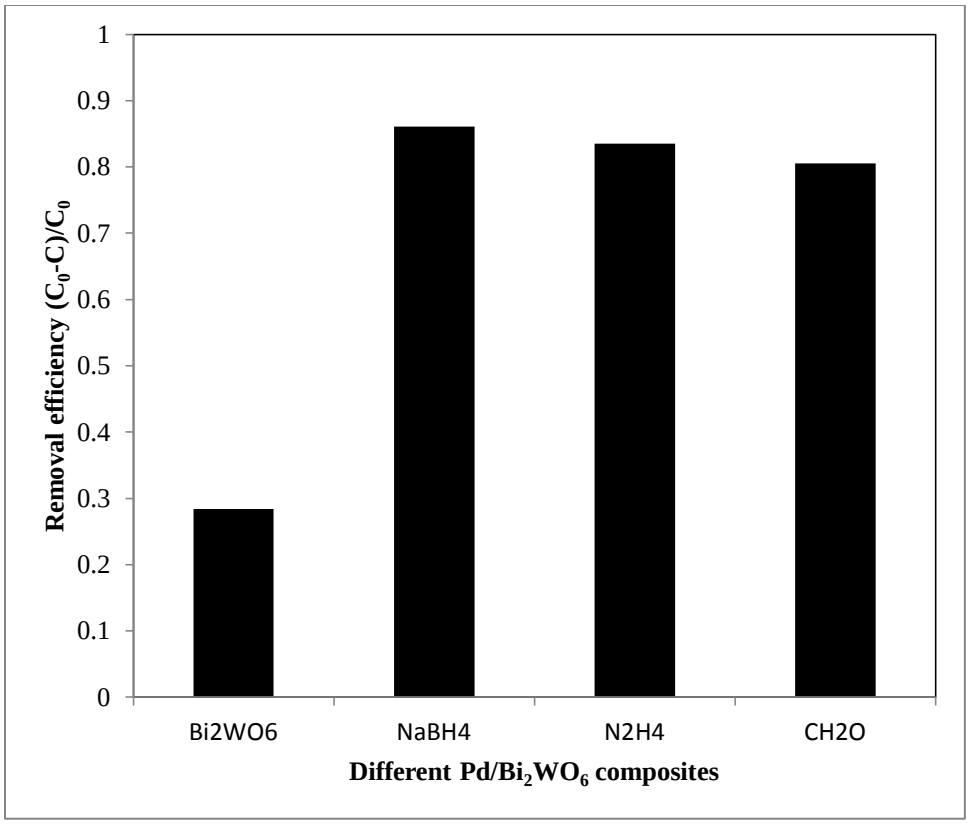

Figure 25 Removal efficiencies of various composites within two hours degradation: (a) pure Bi_2WO_6 (b) $NaBH_4$ reduced composite (c) N_2H_4 reduced composite (d) CH_2O reduced composite

The removal efficiencies of each sample are shown in Figure 24 and Figure 25. In this study, no obvious degradation was observed in the dark and light controls (adsorption only and photolysis only, respectively), indicating that the dye was stable under visible light irradiation, and absorption of RhB had a negligible impact on reaction after the adsorption-desorption equilibrium were achieved. The removal efficiency observed by the samples prepared using $NaBH_4$ exhibited a higher degradation efficiency compared with those obtained using CH_2O and N_2H_4. This phenomenon was thought to be related to different factors, such as the specific surface area, recombination rate of the electron-hole pairs and surface plasmon resonance of Pd nanoparticles under visible light irradiation [1].

The small size of the synthesized particles played a significant role in reducing the pathway from the active site of generation of the electron-hole pairs to the photocatalyst surface. Therefore, the samples prepared using $NaBH_4$ had a slightly higher surface area and lower particle size, and could exhibit increased photocatalytic activity compared to the samples prepared by N_2H_4 and CH_2O. This also corresponded to the results observed by the SEM images which showed the smallest particle size and largest surface areas were obtained with the composite reduced by $NaBH_4$.

4.3.6 Apparent photonic efficiency

The apparent photonic efficiency was introduced because it is a useful tool that rendered the comparison of process efficiencies using different photocatalyst samples. The apparent photonic efficiency was given as a ratio of the reaction rate and the incident light intensity with assumed constant reaction conditions. The apparent photonic efficiency was calculated as the ratio of the number of molecules of reactant consumed per unit time to the number of photons incident in the slurry reactor.

$$\xi = \frac{V\Delta c}{JA\Delta t} \quad (1)$$

where V is the volume (m^3), ξ is the apparent photonic efficiency (mol/ Einstein), Δc is the change in the concentration, J is the flux of photons (Einstein/m^2/s), A is the illuminated area (m^2) and Δt is the change in time [31]. In our research, the quantum meter was used to measure the amount of delivered photons in the range of 400 nm to 700 nm. Due to the illumination used, the actual photons delivered to the reactor were in a larger range than measured. Another limitation is that the concentration was not linear with time so that the corresponding photonic efficiency is variable. Because of the concentration was found to vary nearly linearly with first 30 minutes of the reaction, we decide to use

this time period for the calculation. The results were shown in Table 6. Compared with the other samples, the relative photocatalytic activities of Pd/Bi_2WO_6 prepared by $NaBH_4$, showed the best photocatalytic activity based on the photonic efficiencies, which corresponded to the results calculated by the Langmuir-Hinshelwood and degradation efficiency expression.

Table 6 Apparent photonic efficiencies for various composites for RhB degradation

Photocatalyst	**Apparent photonic efficiency (%)**
Pure Bi_2WO_6	0.542
CH_2O-reduced composite	3.301
N_2H_4-reduced composite	3.423
$NaBH_4$-reduced composite	3.456

4.3.7 Photocatalytic mechanism

Possible mechanisms have been proposed for degradation of Rhodamine B by photocatalysis, as shown in Figure 26. In this scheme, semiconductors are excited by light which has a greater energy than their band gap energy. This causes the production of the excited electron in the conduction band and corresponding positive hole in the valence band. However, the photocatalytic efficiency depends on the competition between the surface charge transfer rate and the quick recombination of photogenerated electrons and the holes. To prevent this recombination, the electrons can easily flow into metal Pd through the Schottky barrier because the conduction band of Bi_2WO_6 is higher than that of the loaded metal Pd. This process of electron transfer is faster than the electron-hole recombination between the valance band and conduction band of Bi_2WO_6. Thus, electrons can be stored in the Pd components. In this scheme, more holes with a strong oxidation power

escape the electron-hole recombination and are available to oxidize the pollutants, which explain why the Pd/Bi_2WO_6 performed with a higher photocatalytic activity than pure Bi_2WO_6 by degradation RhB. The mechanism of $NaBH_4$ reduced composite degradation of RhB dye under visible light irradiation is as follows [32],

$$Bi_2WO_6 + h\nu \rightarrow Bi_2WO_6\,(h^+) + Bi_2WO_6\,(e^-) \quad (1)$$

$$e^- + O_2 \rightarrow O_2^{-\bullet} \quad (2)$$

$$e^- + Pd \rightarrow Pd\,(e^-) \quad (3)$$

$$Pd(e^-) + O_2 \rightarrow Pd + O_2^{-\bullet} \quad (4)$$

$$RhB + O_2/O_2^{-\bullet} \rightarrow \text{products} \quad (5)$$

$$RhB + h^+ \rightarrow \text{products} \quad (6)$$

Because the metallic Pd and Pd ions simultaneously existed in the CH_2O and N_2H_4 reduced composite, reactions (3), (4), (5) and (6) all happened during the degradation process. The mechanism of CH_2O-and N_2H_4-reduced composite degradation of RhB under visible light irradiation is shown below [24].

$$Bi_2WO_6 + h\nu \rightarrow Bi_2WO_6\,(h^+) + Bi_2WO_6\,(e^-) \quad (1)$$

$$e^- + O_2 \rightarrow O_2^{-\bullet} \quad (2)$$

$$e^- + Pd \rightarrow Pd\,(e^-) \quad (3)$$

$$Pd(e^-) + O_2 \rightarrow Pd + O_2^{-\bullet} \quad (4)$$

$$e^- + Pd(\text{II})Cl_2 \rightarrow Pd(\text{I})Cl_2 \quad (5)$$

$$Pd(\text{I})Cl_2 + O_2 \rightarrow Pd(\text{II})Cl_2 + O_2^{-\bullet} \quad (6)$$

$$RhB + O_2/O_2^{-\bullet} \rightarrow \text{products} \quad (7)$$

$$RhB + h^+ \rightarrow \text{products} \quad (8)$$

The absorption band of RhB located at 552 nm is due to the presence of four ethylated

groups attached to the heterocyclic rings structure. When the mixture of photocatalyst and the RhB solution were exposed to light irradiation, the absorption decreased and the peak wavelength moved to the shorter lengths with higher absorption of the dye. Upon the action of formed •OH radicals, the formation of de-ethylated intermediates of the initial molecule gradually decoloured the dye [1].

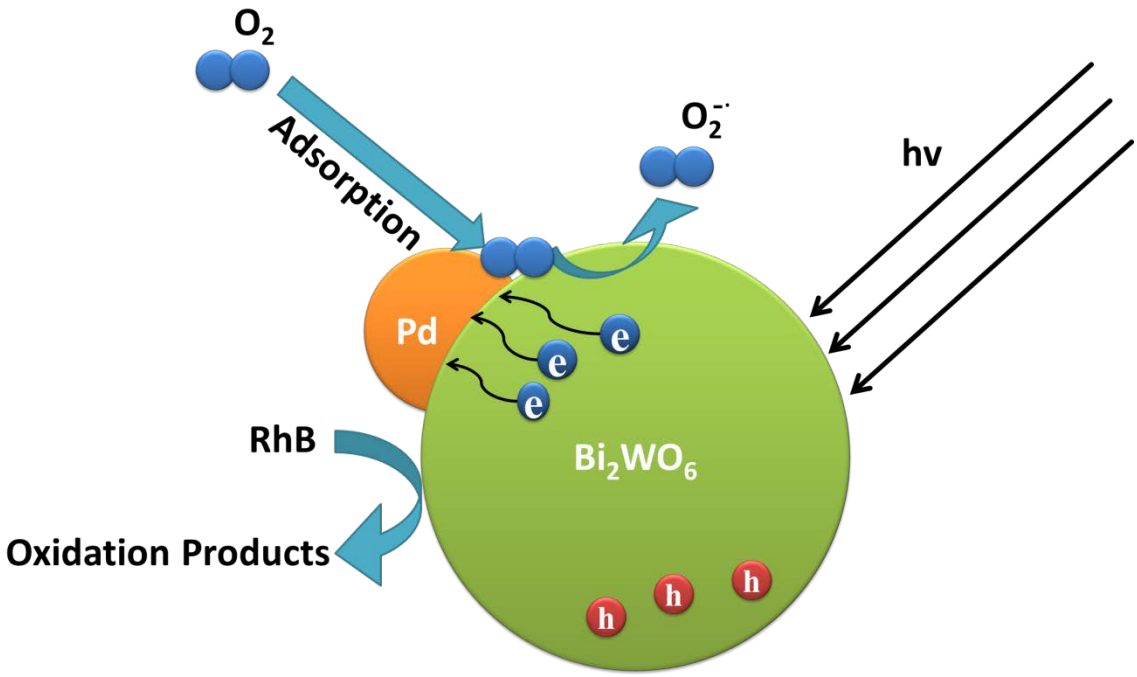

Figure 26 Possible mechanism of degradation of rhodamine B in the presence of Pd/Bi_2WO_6 under visible light irradiation

4.4. Conclusion

In summary, Pd/Bi_2WO_6 was successfully synthesized through a three step process involving hydro-thermal synthesis, isometric impregnation and chemical reduction. Compared to the bare Bi_2WO_6 photocatalyst, the photocatalytic activity of Pd-loaded composites was obviously enhanced for the degradation of RhB under visible light irradiation.

According to the RhB degradation results, the samples prepared using a $NaBH_4$ reductant showed a better degradation capacity than the samples prepared by N_2H_4 and CH_2O. This phenomenon can be related to different factors, such as specific surface area, recombination rate of the electron-hole pairs and surface plasmon resonance of Pd nanoparticles under visible light irradiation. The Pd deposited on the surface of Bi_2WO_6 and did not alter the crystal structure of Bi_2WO_6. The Pd species loaded on Bi_2WO_6 was reduced by chemical reducing agents $CH_2O$and N_2H_4, and was present in the form of both metallic and ionic Pd species (Pd^0 and Pd^{2+}), while the $NaBH_4$-reduced composite contained only metallic Pd species (Pd^0). The composites were shown to degrade RhB under visible light irradiation for two hours, achieving a maximum removal efficiency of 86.1%. It was found that the samples reduced by $NaBH_4$ displayed the highest photocatalytic activity. Future work involves the investigation and characterization of surface area, suspension stability and surface charge data and discernment of their respective impacts on activity. Additionally, the characterization of the photoactivity under real sun or solar simulated irradiation should be conducted to confirm the practical applicability of the photocatalysts.

4.5. References

[1] S. Alfaro, A. Cruz, Synthesis, characterization and visible-light photocatalytic properties of Bi_2WO_6 and $Bi_2W_2O_9$ obtained by co-precipitation method, Applied Catalysis A: General 383 (2010) 128-133.

[2] N. Kim, R. Vannier, C.P. Grey, Detecting Different Oxygen-Ion Jump Pathways in Bi_2WO_6 with 1- and 2-Dimensional ^{17}O MAS NMR Spectroscopy, Chemistry of Materials 17(2005)1925-1958.

[3] P.S. Berdpmsov, D.O. Charkin, V.A. Dolgikh, S.Yu. Stefanovich, R.I. Smith, P. Lightfoot, $Bi_{2-x}Ln_xWO_6$: A novel layered structure type related to the Aurivillius phases, Journal of Solid State Chemistry 177(2004) 2632-2634

[4] L. Zhang, H. Wang, Z. Chen, P. Wong, J. Liu, Bi_2WO_6 micro/nano-structures: synthesis, modifications and visible-light-driven photocatalytic applications, Applied Catalysis B; Environmental 106 (2011)1-13.

[5] Y. Tian, G. Hua, W. Xu, N. Li, M. Fang, L. Zhang, Bismuth tungstate nano/microstructures: Controllable morphologies, growth mechanism and photocatalytic properties, Journal of Alloys and Compounds 509 (2011) 724-730.

[6] S. Zhang, J. Shen, H. Fu, W. Dong, Z. Zheng, L. Shi, Bi_2WO_6 photocatalytic films fabricated by layer-by-layer technique from Bi_2WO_6 nanoplates and its spectral selectivity, Journal of Solid State Chemistry 180 (2007) 1456-1463.

[7] S. Sun, W. Wang, J. Xu, L. Wang, Z. Zhang, Highly efficient photocatalytic oxidation of phenol over ordered mesoporous Bi_2WO_6, Applied catalysis B: Environmental 106 (2011) 559-564.

[8] Y. Liao, J. Wang, J. Lin, W. Chung, W. Lin, C. Chen, Synthesis, photocatalytic activi-

ties and degradation mechanism of Bi_2WO_6 toward crystal violet dye, Catalysis Today 174 (2011) 148-159.

[9] X. Zhang, Y. Zhang, X. Quan, S. Chen, Preparation of Ag doped $BiVO_4$ film and its enhanced photoelectrocatalytic (PEC) ability of phenol degradation under visible light, Journal of Hazardous Materials 167 (2009) 911-914.

[10] J. Colmenares, A. Magdziarz, M. Aramendia, A. Marinas, J. Marinas, F. Urbano, J. Navio, Influence of the strong metal support effect (SMSI) if Pt/TiO_2 and Pd/TiO_2 systems in the photocatalytic biohydrogen production from glucose solution, Catalysis Communications 16 (2011) 1-6.

[11] M. Shang, W. Wang, L. Zhang, S. Sun, L. Wang, L. Zhou, 3D Bi_2WO_6/TiO_2 hierarchical heterostructure: Controllable synthesis and enhanced visible photocatalytic degradation performances, Journal of Physical Chemistry C 113(2009) 14727-14731.

[12] Q. Xiao, J. Zhang, C. Xiao, X.K. Tan, Photocatalystic degradation of methylene blue over Co_3O_4/Bi_2WO_6 composite under visible light irradiation, Catalysis Communications 9 (2008) 1237-1253.

[13] L. Zhang, W. Wang, M. Shang, S. Sun, J. Xu, Bi_2WO_6@carbon/Fe2O4 microspheres: Preparation, growth mechanism and application in water treatment, Journal of Hazardous Materials 172 (2009) 1193-1197.

[14] L. Zhang, K. Wong, Z. Chen, J. Yu, J. Zhao, AgBr-Ag-Bi_2WO_6 nanojunction system: A novel and efficient photocatalyst with double visible-light active components, Applied Catalysis A: General 363 (2009) 221-229.

[15] J. Ren, W. Wang, S. Sun, L. Zhang,J. Chang, Enhanced photocatalytic activity of Bi_2WO_6 loaded with Ag nanoparticles under visible light irradiation, Applied Catalysis B:

Environmental 92 (2009) 50-55.

[16] J. Chae, S. Jung, S. Choi, Synthesis of Au@CSCB and Au@HSPB catalysts by γ-irradiation and chemical reduction, Current Applied Physics 10 (2010) s97-s101.

[17] M.Fox, M. Dulay, Heterogeneous photocatalysis, Chemical Reviews 93 (1993) 341-357.

[18] J. He, I. Ichinose, T. Kunitake, A. Nakao, In situ synthesis of noble metal nanoparticles in ultrathin TiO_2-gel films by a combination of ion-exchange and reduction process, Langmuir 18 (2002) 10005-10010.

[19] J. Ryu, S. Jung, K. Sim, S. Choi, Synthesis of Pt-Ru@PThB catalyst by γ-irradation and $NaBH_4$ as reducing agent, Applied Radiation and Isotopes 67 (2009) 1449-1453.

[20] J. Hajek, P. Maki-arvela, E. Toukoniitty, N. Kumar, T. Salmi, D. Murzin, The effect of chemical reducing agents in the synthesis of sol-gel Ru-Sn catalysts: selective hydrogenation of Cinnamaldehyde, Journal of Sol-Gel Science and Technology 30 (2004) 187-195.

[21] Z. Zhang, W. Wang, M. Shang, W. Yin, Low-temperature combustion synthesis of Bi_2WO_6 nanoparticles as a visible-light-driven photocatalyst, Journal of Hazardous Materials 177 (2010) 1013-1018.

[22] F. Duan, Y. Zheng, M. Chen, Flowerlike $PtCl_4/Bi_2WO_6$ composite photocatalyst with enhanced visible-light-induced photocatalytic activity, Applied Surface Science 257 (2011) 1972-1978.

[23] L. Ge, Synthesis and characterization of novel visible-light-driven $Pd/BiVO_4$ composite photocatalysts, Materials Letters 62 (2008) 926-928.

[24] J. Domaradzki, Structural, optical and electrical properties of transparent V and

Pd-doped TiO_2 thin films prepared by sputtering, Thin solid films 497 (2006) 243-248.

[25] L. Wu, J. Bi, Z. Li, X. Wang, X. Fu, Rapid preparation of Bi_2WO_6 photocatalyst with nanosheet morphology via microwave-assisted solvothermal synthesis, Catalysis today 131 (2008) 15-20.

[26] Q. Xiao, J. Zhang, C. Xiao, X. Tan, Photocatalytic degradation of methylene blue over Co_3O_4/Bi_2WO_6 composite under visible light irradiation, Catalysis Communications 9 (2008) 1247-1253.

[27] D Wang, G. Xue, Y. Zhen, F. Fu, D. Li, Monodispersed Ag nanoparticles loaded on the surface of spherical Bi_2WO_6 nanoarchitectures with enhanced photocatalytic activities, Journal of material chemistry 22 (2012) 4751-4758.

[28] C. Xiao, C. Shen, Z. Xu, T. Yang, H. Gao, Anomalous aggregation growth of palladium nanosphere with SPR band in visible range, Chinese physics B 17 (2008) 2066-2071.

[29] A. Kanchana, S. Devarajan, S. Ayyappan, Green synthesis and characterization of palladium nanoparticles and its conjugates from solanum trilobatum leaf extract, Nano-micro letters 2 (2010) 169-176.

[30] J. Herrmann, Heterogeneous photocatalysis: fundamentals and applications to the removal of various types of aqueous pollutants, Catalysis Today 53 (1999) 115-129.

[31] H. Fu, C. Pan, W. Yao, Y. Zhu, Visible-Light-Induced Degradation of Rhodamine B by Nanosized Bi_2WO_6, The journal of physical chemistry B 109 (2005) 22432-22439.

[32] D. Wang, G. Xue, Y. Zhen, F. Fu, D. Li, Monodispersed Ag nanoparticles loaded on the surface of spherical Bi_2WO_6 nanoarchitectures with enhanced photocatalystic activities. Journal of Materials Chemistry 22 (2012) 4751-4758.

Chapter 5. Conclusions and future works

5.1. Summary and conclusions

$PdCl_2/Bi_2WO_6$ and Pd/Bi_2WO_6 hierarchical nanoparticles were successfully synthesized via a template free hydrothermal process and their photocatalytic activities were investigated by degradation of Rhodamine B. The $PdCl_2/Bi_2WO_6$ and Pd/Bi_2WO_6 composites were characterized by X-ray diffraction (XRD), scanning electron microscopy (SEM), X-ray photoelectron spectroscopy (XPS) and ultraviolet visible (UV-vis) light diffuse reflectance spectra, respectively.

Rhodamine B degradation studies revealed that $PdCl_2/Bi_2WO_6$ exhibited a higher photocatalytic activity compared to the pure Bi_2WO_6, because of the synergetic effect between the transition metal Pd and semiconductor. By XRD, XPS and SEM observations, it was found that the deposition of Pd species did not affect the crystal lattice of Bi_2WO_6 photocatalyst. When the pH value was equal to 4, 100 mg/L RhB solution was photodegraded by 4 g/L of $PdCl_2/Bi_2WO_6$ after one hour of visible light irradiation, and 1 wt% $PdCl_2/Bi_2WO_6$ photocatalyst exhibited an optimum value of the photocatalytic efficiency of 97.5%.

Composite Pd/Bi_2WO_6 was successfully synthesized through a three step process involving hydro-thermal synthesis, isometric impregnation and chemical reduction. Compared to the bare Bi_2WO_6 photocatalyst, the photocatalytic activity of Pd-loaded composites was obviously enhanced for the degradation of RhB under visible light irradiation. According to the RhB degradation results, the samples prepared using a $NaBH_4$ reductant

showed a better degradation capacity and optical absorption property than the samples prepared by N_2H_4 and CH_2O. The Pd species loaded on Bi_2WO_6 were reduced by chemical reducing agents CH_2O and N_2H_4, and was present in the form of both metallic Pd and Pd ion species (Pd^0 and Pd^{2+}), while the Pd species in $NaBH_4$ reduced composite contained only metallic Pd species (Pd^0). The photocatalytic activities of chemically reduced Pd/Bi_2WO_6 composites were quantified by the degradation of RhB under visible light, and a maximum removal efficiency of 86.1% was obtained after 2 hours of irradiation. $PdCl_2/Bi_2WO_6$ exhibited higher photocatalytic activity than $NaBH_4$-, CH_2O- and N_2H_4-reduced Pd/Bi_2WO_6 composites, and this was thought to be attributable to the following factors:

1. From the SEM images observed, the particle size of $PdCl_2/Bi_2WO_6$ photocatalysts was smaller than the reduced Pd/Bi_2WO_6. Higher surface area and smaller particle size would have played a role in increasing the photocatalytic activity [1].

2. Pd species reduced by chemical reductants led to the aggregation of metallic nanoparticles on the surface of Bi_2WO_6, which decreased the specific surface areas and covered the active sites on Bi_2WO_6 surface. Chen et al. reported that the major drawback of using chemical reactants was the difficulty in controlling the particle size and dispersion [2].

3. The loaded Pd species may also have been leached off during the chemical reduction process, leading to the decrease in the photocatalytic activity [3].

5.2. Future work

The following studies are recommended:

1. The investigation and characterization of surface area, suspension stability and their respective impacts on activity should be discerned.

2. The characterization of the photocatalytic activities under real sun or solar simulated irradiation should be conducted to confirm the practical applicability of the photocatalyst.

3. The loading of other noble metal on Bi_2WO_6 such as Pt, Ru and Au should be investigated, and their structure and photocatalytic activity studied

4. The feasibility of integration of the photocatalytic material with photocatalytic generator or solar cell for large-scale commercial treatment should be assessed.

5.3. References

[1] S. Alfaro, A. Cruz, Synthesis, characterization and visible-light photocatalytic properties of Bi_2WO_6 and $Bi_2W_2O_9$ obtained by co-precipitation method, Applied Catalysis A: General 383 (2010) 128-133.

[2] J. Chen, C. Jiang, X. Yang, L. Feng, E. Gallogly, R. Wang, Studies on how to obtain the best catalytic activity of Pt/C catalyst by three reduction routes for methanol electro-oxidation, Electrochemistry Communications 13 (2011) 314-316.

[3] L. Cerveny, I. Paseka, E. Laine, The effect of chemical reducing agents in the synthesis of sol-gel Ru-Sn catalysts: selective hydrogenation of cinnamaldehyde, Journal of sol-gel and technology 30 (2004) 187-195.

APPENDICES

Appendix A. Calibration curve between the dye concentration and the light intensity at a wavelength of 520 nm measured using a spectrophotometer.